Catalytic site ensembles: A context to reexamine the Langmuir-Hinshelwood kinetic description

Authors: N. K. Razdan[1], A. Bhan[1]*

Affiliations

[1]Department of Chemical Engineering and Materials Science, University of Minnesota-Twin Cities, 421 Washington Avenue SE, Minneapolis, Minnesota 55455, United States.

*Correspondence to: abhan@umn.edu; Fax: (+1) 612-626-7246.

Abstract

The Langmuir-Hinshelwood formalism describes catalytic reactions of Langmuirian surface species under the assumption that all adsorbates are randomly-distributed – enabling adjacency of surface-bound intermediates to be determined solely by coverages of single-site occupants. We demonstrate herein that this approximation is inappropriate even for simple catalytic reactions (e.g. $A + A \rightarrow A_2$) and manifestly neglects islanding of slowly-consumed species and partitioning of highly-reactive species inherently engendered by ≥two-site elementary steps (e.g. $A^*–A^* \rightarrow A_{2(g)} + *–*$). Rigorous description of kinetically-consequential islanding/partitioning phenomena requires explicit description of the coverage and chemical dynamics of all multi-site ensembles. Higher-order, ensemble-specific rate terms identify the particular microscopic events relevant to each ensemble, and, in doing so, reveal that each elementary step (e.g. $A_{(g)}$ adsorption) describes not one event (e.g. $A_{(g)} + * \rightarrow A^*$) , but a sum over all ensemble-specific paths (e.g. $A_{(g)} + *–* \rightarrow A^*–*$ and $A_{(g)} + A^*–* \rightarrow A^*–A^*$). De-convoluting each elementary step into its constituent multi-site paths proffers kinetic detail otherwise inaccessible – enabling (i) identification of rate- and selectivity-determining site ensembles, (ii) calculation of rates and degrees of rate control of ensemble-specific elementary steps, (iii) incorporation of adsorbate surface diffusion, (iv) incorporation of lateral adsorbate interactions, and (v) quantitative description of catalysis of multi-site-occupying intermediates (e.g. $^*C_nH_m^*$ species in hydrocarbon (de-)hydrogenation and *C-C* bond coupling/cleavage reactions) which we demonstrate is inaccessible to the Langmuir-Hinshelwood formalism even if adsorbate surface diffusion is infinitely-fast.

Keywords: Catalytic site ensembles, surface diffusion, lateral adsorbate interactions, coverage-dependent rates, transition-state theory

1. Introduction

Catalytic sequences on surfaces with elementary steps that require multiple sites (e.g. H_2 + *–* ⇌ H^*–H^*) are sensitive to the concentration and distribution of multi-site ensembles (e.g. *–* and H^*–H^*). Non-random adsorbate distribution, characterized by clustering or isolation of surface species, profoundly affects reaction kinetics and controls relative propagation of competing reaction paths proceeding through ensembles of disparate size and/or composition. Distinct ensemble site requirements of competing pathways has been leveraged to control selectivity in alkene epoxidation/oxidation [1,2], alkane (de-)hydrogenation/hydrogenolysis [3,4], and oxygenate dehydrogenation/dehydration [5] by judicious introduction of poisons or promoters which regulate the assembly of selectivity-determining ensembles. Pre-eminent mean-field kinetic models such as the Langmuir-Hinshelwood formalism have experimentally [6–8] and computationally [9–11] been demonstrated to be incapable of accurately describing such ensemble (i.e. geometric) effects due to an inability to explicitly enumerate populations of multi-site ensembles on which elementary steps occur. Miscounting of ensemble coverages consequents miscalculation of reaction rates, reaction orders, and degrees of rate control – resulting in a kinetic description unreliable for mechanistic interpretation (e.g. rationalization of observed reaction kinetics) or comparison with *ab initio* calculation of kinetic parameters (e.g. by DFT, density functional theory) [9,10,12].

This work is dedicated to description and explication of a mathematical framework which explicitly enumerates ensembles of any size, shape, and composition and, in doing so, redresses the principal shortcoming of the Langmuir-Hinshelwood formalism. As a means of introduction to the mathematical treatment to follow, we first define the Langmuir-Hinshelwood kinetic description and detail the manner by which the method miscounts multi-site ensembles.

The Langmuir-Hinshelwood method describes catalytic surface reactions of adsorbed species obeying the conditions of the Langmuir theory of adsorption:

(I) The adsorbent/catalytic surface is a defect-free, flat 2D lattice

(II) Each site is either vacant or occupied by at most one adspecies

(III) Each site is energetically identical and adsorbates have no energetic interactions. We refer to this as the system being *thermodynamically-ideal*.

Provided all elementary steps require only a single catalytic site, no further conditions are required to construct an analytical kinetic description of sorption/reaction of Langmuirian surface species. Many catalytic reaction sequences, however, involve ≥two-site elementary steps such as dissociative adsorption (H_2 + *–* ⇌ H^*–H^*), the rate of which is determined by coverages of the requisite multi-site ensembles. The Langmuir-Hinshelwood formalism addresses this complication by application of the Hinshelwood approximation:

(IV) The spatial distribution of adsorbates is random (i.e. there are no spatial correlations between sites). We refer to this as the system being *combinatorially-ideal* or *configurationally-ideal*.

The utility of the Hinshelwood approximation is in reducing coverages of multi-site ensembles to a product of coverages of the constituent single-site occupants [10,13,14]. That is to say, for example, that the fractional coverage of H^*–H^* pairs, $\theta_{H^*-H^*}$, is assumed equal to $\theta_{H^*}^2$. This simplifying approximation is ubiquitous and foundational to catalytic kinetic formalisms of Boudart and Djéga-Mariadassou [15], Hill [16], and Hougen and Watson [17] – all of which are modified variants or particular representations of the Langmuir-Hinshelwood kinetic description. The Hinshelwood approximation, however, evidently neglects the possibility of configurational biasing manifest as H^* islanding ($\theta_{H^*-H^*} > \theta_{H^*}^2$) or partitioning ($\theta_{H^*-H^*} < \theta_{H^*}^2$) which inherently

accompanies any reaction sequence comprised of elementary steps requiring two or more sites, even in the absence of thermodynamic non-idealities (e.g. lateral adsorbate interactions) [10–12]. The principal development of this work is to provide an analytical framework which improves upon the spatial myopia of the Hinshelwood approximation, enabling explicit retention of multi-site coverages such as $\theta_{H^*-H^*}$ as independent variables with unique, coverage-dependent elementary step rates.

The Langmuir-Hinshelwood kinetic formalism, and variants thereof (e.g. Langmuir-Hinshelwood-Hougen-Watson models [17]), do not retain terms such as $\theta_{H^*-H^*}$ and, consequently, are only reliable for description of catalytic reactions of Langmuirian adsorbates if adspecies surface diffusion is rapid compared to catalysis and thusly randomizes the adsorbate distribution – a condition which is not ensured by (quasi-)equilibration of sorption steps [12] and which is prohibited by the presence of multi-site occupying species (e.g. two-site occupying $^*C_2H_4^*$ in catalytic (de-)hydrogenation [18]) as detailed in Case Study III herein. Accurate kinetic description of configurational non-idealities imperceptible to the Langmuir-Hinshelwood formalism requires relaxation of the Hinshelwood mean-field approximation (IV) to quantify the effect of adspecies islanding/partitioning phenomena on rates, selectivities, and elementary step activation energies.

We recently developed a formalism which explicitly describes dynamics of multi-site ensembles by inclusion of higher-order rate terms specific to each ensemble and each elementary step [12]. Coverage-dependent, ensemble-specific rate terms reveal that each elementary step cannot be wholly described by a single rate expression, rate constant, and reversibility; instead, each multi-site ensemble is associated with a unique rate for each elementary step – the collection of which describes a distinct, ensemble-specific path from reactants to products.

Remarkably, even single-site elementary steps require a unique kinetic description for each ensemble.

Consider, for example, the adsorption of gas-phase $A_{(g)}$ onto a vacant site

$$A_{(g)} + * \rightleftharpoons A^* \quad \textbf{[1]}$$

The rate with respect to single-site ensembles follows directly from the law of mass action

$$r_{ads,[A^*]} = -r_{ads,[*]} = k_{ads} a_A \theta_* - k_{des} \theta_{A^*} \quad \textbf{[2]}$$

where $r_{ads,[i]}$ is the rate of adsorption with respect to site occupant i, a_A is the thermodynamic activity of $A_{(g)}$, k_{ads} and k_{des} are the rate constants of adsorption and desorption, respectively, and θ_i is the fractional coverage of site occupant i. The rate with respect to site pairs, however, depends on the occupation of sites neighboring each adsorption center; A^*–A^* pairs, for example, are only generated by adsorption events such as $A_{(g)} + A^*–* \rightarrow A^*–A^*$, the rate of which is determined by the two-site fractional coverage $\theta_{A^*–*}$. Quantitative definition of such two-site coverages, neglected in the Langmuir-Hinshelwood formalism, requires account of statistical factors pertaining to lattice coordination, c, and inherent two-site occupancy of site pairs

$$\theta_{ij} \equiv \frac{N_{ij}}{N_{pairs}} = \frac{N_{ij}}{N_{sites}\left(\frac{c}{2}\right)} \quad \textbf{[3]}$$

where N_{ij} is the number of ij pairs, N_{pairs} is the total number of pairs, N_{sites} is the total number of sites, and $c = 4$ for a 2D square lattice. In comparison, definition of single-site coverages requires no consideration of lattice coordination (i.e. $\theta_i \equiv N_i/N_{sites}$).

We note that Eq. **3** follows the convention that heterogeneous ensembles are distinguishable and of equal population [19–21]. That is to say ij and ji pairs are distinct, $\theta_{ij} = \theta_{ji}$, and $(\theta_{ij})_{max} = (\theta_{ji})_{max} = ½$. This convention is distinct from that of Boudart and Djéga-Mariadassou [15] and is chosen so that (i) $\theta_{ij} = \theta_{ji} = \theta_i\theta_j$ for a random adsorbate distribution and (ii) the i species balance

is $\theta_i = \Sigma_j\, \theta_{ij}$. Boudart and Djéga-Mariadassou [15], Hougen and Watson [17], and Zhdanov [22] consider *ij* and *ji* pairs indistinguishable, giving (i) $\theta_{ij} = (2 - \delta_{ij}) \times \theta_i\theta_j$ for a random adsorbate distribution and (ii) species balance $\theta_i = \Sigma_j\, \theta_{ij} \times (2 - \delta_{ij})^{-1}$ where δ_{ij} is the Kronecker delta. As the mathematical treatment to follow will demonstrate, the convention distinguishing *ij* and *ji* pairs which we adopt – absent δ_{ij} terms – is particularly conducive for physical interpretation of the concentration, distribution, and kinetic relevance of homogeneous and heterogeneous ensembles alike.

Scheme 1 provides visualization of the definition of θ_{ij} in Eq. **3** by enumeration of all one- and two-site ensembles on a 3 × 3 square lattice with periodic boundaries. The visual aid identifies all ½c × (3 × 3) = 18 site pairs and, in doing so, calculates $\theta_{A^*\text{–}A^*}$, $\theta_{*\text{–}*}$, and $\theta_{A^*\text{–}*} = \theta_{*\text{–}A^*}$ which do not conform to the generally unreliable Hinshelwood approximation. We encourage the reader to follow and/or reproduce enumeration of site ensembles in Scheme 1 to ensure the theory and results hereinafter are interpreted in the appropriate context.

Scheme 1: Illustrative enumeration of two-site ensembles†

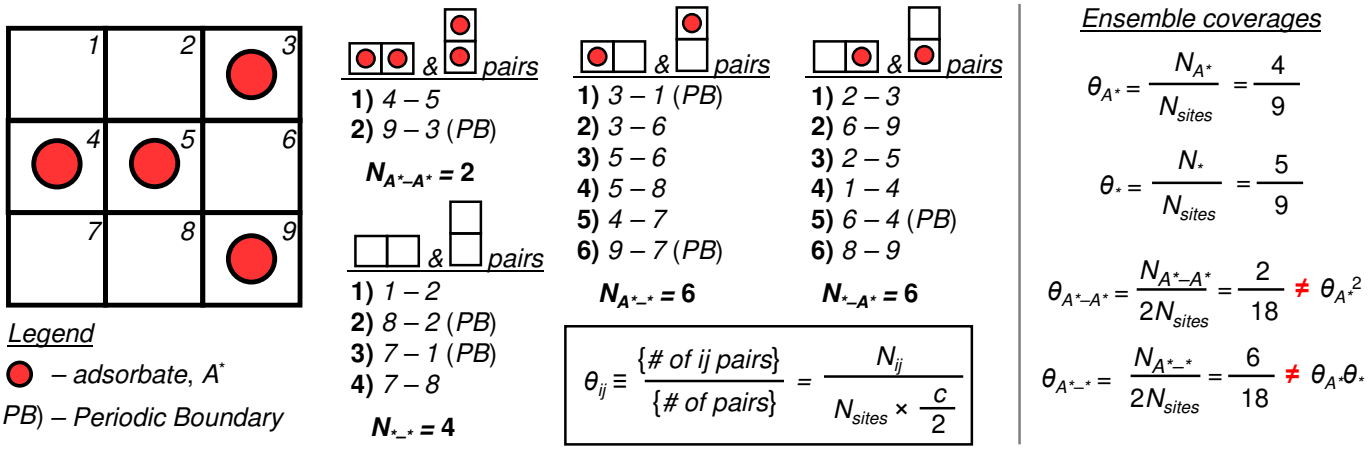

†Lattice sites are either vacant, *, or occupied by adsorbate A^* (●). Each lattice site is numbered for identification of all 18 site pairs as A^*–A^*, A^*–*, *–A^* or *–*. The coordination number, c, is equal to 4 on a square lattice. Edge sites are subject to periodic boundaries such that sites *6* and *4*, for example, are considered nearest neighbors.

Definition of two-site ensemble coverages in hand, we derive ensemble-specific $A_{(g)}$ sorption rate equations with aid of Scheme 2 which illustrates enumeration of the sorptive configurations

relevant to the population of each site pair. Consider, for example, the rate of adsorption with respect to the A^*–A^* ensemble, $r_{ads,[A^*-A^*]}$, shown in the second row of Scheme 2. Enumeration of the relevant sorptive configurations reveals that all sorption events which generate/eliminate A^*–A^* pairs are elementary steps of the form

$$A_{(g)} + A^* - * \rightleftharpoons A^* - A^* \quad \textbf{[4]}$$

which, per the law of mass action, gives

$$r_{ads,[A^*-A^*]} = 2k_{ads}a_A\theta_{A^*-*} - 2k_{des}\theta_{A^*-A^*} \quad \textbf{[5]}$$

where the statistical factor of '2' accounts for the two distinct adsorptive configurations, *–A^* and A^*–*, which can generate A^*–A^* pairs. Similarly, *–* pairs are generated by desorption from both *–A^* and A^*–* pairs, giving analogous statistical factors of '2'

$$r_{ads,[*-*]} = -2k_{ads}a_A\theta_{*-*} + 2k_{des}\theta_{A^*-*} \quad \textbf{[6]}$$

because of the two mirror-image microscopically-reversible sorption events which generate/eliminate *–* pairs (see bottom row of Scheme 2). Sorption rate equations for the heterogeneous ensemble A^*–* are absent the statistical factor '2'

$$r_{ads,[A^*-*]} = k_{ads}a_A(\theta_{*-*} - \theta_{A^*-*}) - k_{des}(\theta_{A^*-*} - \theta_{A^*-A^*}) \quad \textbf{[7]}$$

because creation/annihilation of the *–A^* pair is irrelevant with the convention of distinguishing *ij* and *ji* pairs. Explicit derivation of sorption rate equations for *–A^* pairs is unremunerative because *–A^* pairs are necessarily always equal in population to A^*–* pairs; therefore, throughout this text, we do not replicate rate equations for *ij* and *ji* pairs.

Scheme 2: Enumeration of two-site adsorption rate equations†

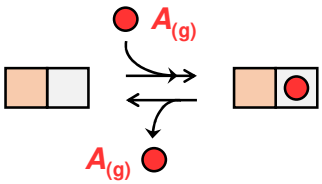

$$r_{ads} = k_{ads}a_A[\square] - k_{des}[\bullet]$$

$$r_{ads,[A^*-A^*]} = k_{ads}a_A[\bullet\square + \square\bullet] - k_{des}[\bullet\bullet + \bullet\bullet]$$

$$r_{ads,[A^*-*]} = k_{ads}a_A[\square\square - \bullet\square] - k_{des}[\bullet\square - \bullet\bullet]$$

$$r_{ads,[*-*]} = -k_{ads}a_A[\square\square + \square\square] + k_{des}[\square\bullet + \bullet\square]$$

†Adsorption of $A_{(g)}$ (●) onto the vacant white lattice site (□) generates adsorbed A^* and creates/eliminates site pairs A^*–A^*, A^*–*, and *–* depending on the occupation of the neighboring lattice site (□).

Eqs. **5** – **7** explicate the provenance of multi-site ensemble-specific rates which enable description of non-idealities in adsorbate distribution inaccessible to the Langmuir-Hinshelwood formalism. We quantify configurational biasing effected by ensemble site requirements by calculation of the mean-field metric

$$\mu_{ij} \equiv \frac{\theta_{ij}}{\theta_i\theta_j} \qquad \textbf{[8]}$$

which is assumed unity in the Langmuir-Hinshelwood method. Deviations from $\mu_{ij} = 1$ quantify the inaccuracy of the Hinshelwood approximation and provide physical insight regarding the clustering and partitioning of each site pair. Similarly, $\mu_{ijk} \equiv \theta_{ijk}(\theta_i\theta_j\theta_k)^{-1}$ quantifies the aggregation and dispersion of three-site ensembles, and so on.

Intuitively, the clustering of one site pair must be counter-balanced by the partitioning of another. This constraint is quantitatively described by combination of overall and component site balances

$$1 = \sum_{\substack{j=site \\ occupants}} \theta_j \qquad \textbf{[9]}$$

and

$$\theta_i = \sum_{\substack{j=site \\ occupants}} \theta_{ij} \qquad \textbf{[10]}$$

where indices *i* and *j* for site occupants include vacant sites, *. Division of Eq. **10** by θ_i gives the mean-field metric balance

$$1 = \sum_{\substack{\mathrm{j=site} \\ \mathrm{occupant}}} \mu_{ij}\theta_j \;\; \forall \;\; \mathrm{i} \qquad \textbf{[11]}$$

which accounts for the necessary concomitance of adsorbate clustering and isolation (i.e. if $\mu_{ij} < 1$ then at least one $\mu_{ik} > 1$). We note that the particular form of the component and mean-field metric balances is predicated on the convention that heterogeneous pairs *ij* and *ji* are distinguishable and of equal population – as is discussed in Eq. **3** and Scheme 1. If heterogeneous pairs *ij* and *ji* are considered indistinguishable, then $(\theta_{ij})_{max} = 1$ and each term in the sum of Eq. **10** must adjoin the multiplicative term $(2 - \delta_{ij})^{-1}$. The chosen convention ensures $\mu_{ij} = 1$ implies combinatorial ideality regardless of homogeneity or heterogeneity of the considered ensemble.

In the absence of thermodynamic non-idealities, adsorbate clustering and isolation is caused by disparate elementary step rates and site-size requirements engendering (i) aggregation ($\mu_{ij} >> 1$) of slowly-consumed ensembles and (ii) partitioning ($\mu_{ij} << 1$) of rapidly-consumed ensembles – resulting in a 'poorly-mixed' or 'transport-limited' surface. Adsorbate surface diffusion resolves rate-controlling 'transport limitations' by dispersing clustered species and allying highly-reactive, isolated species. In the limit of infinitely-fast surface diffusion (i.e. a reaction-limited, rather than transport-limited surface), adsorbate distribution randomizes and the Hinshelwood approximation becomes valid – save for catalytic surfaces populated by multi-site occupying adsorbates (e.g. $^{*}C_2H_4^{*}$) as discussed in Case Study III (*vide infra*).

Our formalism quantitatively accounts for the effects of surface diffusion in redressing poor 'surface mixing' and identifies compendious kinetic descriptors inaccessible to the Langmuir-Hinshelwood formalism or lattice-based kinetic Monte Carlo (kMC) simulation. Retention of higher-order rate terms, analogous to those derived in Scheme 2, reveal each ensemble experiences a unique elementary diffusion event, analogous to the ensemble-specific elementary adsorption event in Eq. **4**. The ensemble-specificity with which each elementary step is described is key to the improvements of higher-order formalisms and enables quantitative identification of hitherto incognizable rate- and selectivity-determining ensembles, as in Case Study I (*vide infra*). The improved descriptive scope proffered by the higher-order formalism is robust to inclusion of lateral adsorbate interactions (see Section 4.2) and non-uniform site distributions (see Section 4.1) in both the rationalization of experimental rate data and the interpretation of *ab initio* calculation of kinetic parameters. In fact, we posit that DFT-generated reaction mechanisms are most appropriately studied either by lattice-based kMC simulation or by higher-order microkinetic models – both of which redress inability of the Langmuir-Hinshelwood method to capture thermodynamic or combinatorial non-idealities.

In what follows, we (i) explicate higher-order descriptions of multi-site elementary steps, (ii) introduce established and novel kinetic descriptors useful for interpretation of catalytic reaction sequences, and (iii) present three case studies which highlight limitations of the Langmuir-Hinshelwood (i.e. zeroth order) formalism and the improved descriptive scope and depth of higher-order formalisms.

The ensemble-specific description of multi-site elementary steps is complicated by the inherent spatial coupling conferred by the reacting/sorbing/diffusing ensemble. Consider, for example, the reaction of two neighboring A^* species to form $A_{2(g)}$

$$A^* - A^* \rightarrow A_{2(g)} + * - * \qquad \textbf{[12]}$$

which occurs with rate

$$-r_{sr,[A^*]} = r_{sr,[*]} = c \cdot k_{sr}\theta_{A^*-A^*} = 4k_{sr}\theta_{A^*-A^*} \qquad \textbf{[13]}$$

where c is the coordination number and c = 4 on a square lattice. As Eq. **13** explicates, the involvement of multiple sites in the surface reaction step consequents a rate with respect to single-site ensembles which necessarily depends on coverages – and therefore rates – of larger ensembles (i.e. θ_{A*-A*}). This complexity – absent in kinetic description of single-site elementary steps (see Eqs. **2**, **5** – **7**) – extends to rate equations for two-site ensembles; for example, the rate of surface reaction with respect to A^*-A^* pairs on a 2D square lattice is

$$-r_{sr,[A^*-A^*]} = k_{sr}\left[\theta_{A^*-A^*} + 2\theta_{A^*-A^*-A^*} + 4\theta_{\substack{A^*-A^* \\ | \\ A^*}}\right] \qquad \textbf{[14]}$$

which is in terms of three-site coverages, as illustrated in Scheme 3. The first term in Eq. **14** accounts for the annihilation of an A^*-A^* pair for each reaction event, and the second and third terms account for additional loss of A^*-A^* pairs if A^* species neighbor the reacting ensemble (e.g. orange (□) and green (□) A^*-occupied sites in Scheme 3). Evidently, the coupling of the reacting ensemble with neighboring sites results in coverage terms for ensembles larger than A^*-A^*. The rate equation for $\theta_{A*-A*-A*}$ similarly couples with ensembles of size four (e.g. $\theta_{A*-A*-A*-A*}$) and so on. The complete kinetic description of multi-site elementary steps is therefore an *infinite* set of hierarchical rate equations describing dynamics of ever-larger ensembles.

Scheme 3: Schematic derivation of ensemble-specific surface reaction rate for A^*-A^* pairs†

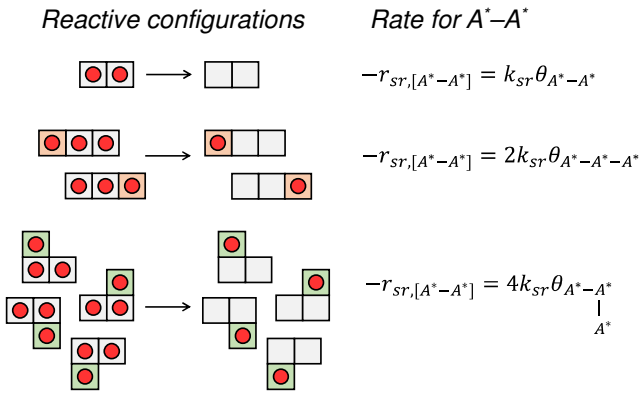

†Surface reaction of two A^* species (●) occupying neighboring white lattice sites (□) eliminates site pairs A^*–A^* with ensemble-specific rate $r_{sr,[A^*-A^*]}$ enhanced by A^*-occupation of neighboring sites forming linear (▭) or bent (▯) three-site configurations.

The unbounded set of hierarchical rate equations is made finite and solvable by a mathematically-rigorous truncation procedure which retains only terms up to a specified order – analogously to the truncation of Taylor series expansions. The complete Taylor series expansion of e^x, for example, is an infinite series $e^x = \Sigma_n\, x^n/n!$ and is only exact in the limit $n \rightarrow \infty$. Retention of terms up to order one, however, (i.e. $e^x = 1 + x$) is, for $x << 1$, sufficiently accurate and deemed the optimum balance of completeness and simplicity. In much the same way, the infinite hierarchy of rate equations is truncated to retain coverage terms up to a specified order – the appropriateness of which is determined by the shape and size of ensembles through which elementary steps proceed.

The truncation of hierarchical, ensemble-specific rate equations operates directly on ensemble site coverages and is detailed in our recent work [12]. Briefly, truncation procedures of order n wholly retain coverages of ensembles wherein each constituent site is separated from every other constituent site by at most n lattice vectors. For example, Scheme 4 illustrates the A^*-covered ensembles wholly retained by the zeroth-, first-, and second-order formalisms. The zeroth-order formalism only explicitly describes ensembles in which all constituent sites are separated by zero lattice vectors – trivially, only single-site configurations – and, therefore, is

exactly the Langmuir-Hinshelwood formalism. Coverages of multi-site ensembles cannot be completely described by the zeroth-order method and are thus reduced to a product of single-site coverages, as shown in Scheme 4(b). Similarly, the first-order formalism can only explicitly describe coverages of one- and two-site ensembles. Larger ensemble coverages – which are retained in the second order – must be reduced to a product/quotient of one- and two-site ensembles coverages, as shown in Scheme 4(b) and explicated in the following section.

Scheme 4: Comparison of zeroth, first, and second order formalisms[†]

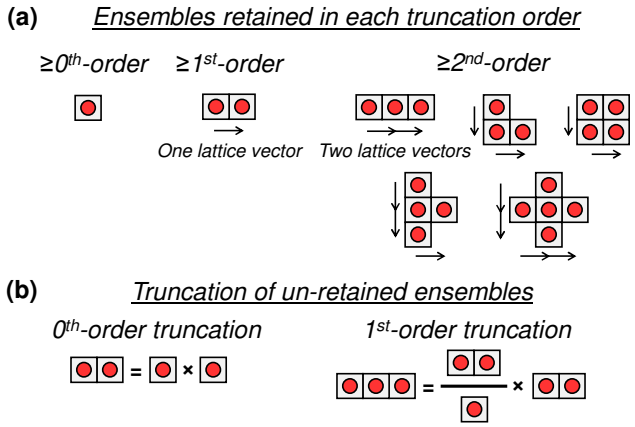

[†](a) A^*-covered ensembles on a 2D square lattice retained in each truncation order. For example, all truncation orders ≥1 retain ensembles of size two. Ensembles wholly retained by truncation orders ≥2 are composed of sites separated by at most two lattice vectors. (b) Ensembles not explicitly retained in a given order must be reduced to a product/quotient of retained ensembles. For example, in the zeroth-order, $\theta_{A^*\_A^*} = \theta_{A^*} \times \theta_{A^*}$ and, in the first-order, $\theta_{A^*\_A^*\_A^*} = (\theta_{A^*\_A^*}/\theta_{A^*}) \times \theta_{A^*\_A^*}$.

In general, propriety of truncation order is determined by the number of lattice vectors needed to wholly retain all ensembles on which elementary steps occur. The first-order formalism is therefore sufficient to accurately describe all catalytic sequences occurring through at most two sites. The Langmuir-Hinshelwood, or zeroth-order, formalism, however, can only reliably describe catalytic sequences involving at most one site and is consequently inappropriate for description of two-site steps such as bimolecular surface reactions (e.g. $N^* + H^* \rightleftharpoons NH^* + *$) [23,24]. Case Studies hereinafter compare zeroth-order, first-order, second-order, and kMC kinetic description of catalytic sequences proceeding through two or more sites to affirm

invalidity of the Langmuir-Hinshelwood formalism and demonstrate quantitative accuracy and profound physical insight conferred by the ensemble-specificity of higher-order analytical descriptions.

2. Methods

2.1 Truncation of hierarchical rate equations

Coverages of ensembles too large to be retained in a specified order must be systematically truncated to a product/quotient of wholly retained ensembles. The truncation procedure, formally detailed in the work of Nord and Evans [19,21,25], operates on conditional probabilities – which we regard best defined by example. Consider the conditional probability, $\chi_{A^*-\alpha^*}$, that a *conditioned* site is A^*-occupied given the neighboring *conditioning* site α^* is A^*-occupied with 100% probability

$$\chi_{A^*-\alpha^*} = \frac{\theta_{A^*-A^*}}{\theta_{A^*}} \qquad \textbf{[15]}$$

As Eq. **15** exemplifies, the conditional probability provides a rigorous relation between ensembles of disparate size and is therefore useful for the truncation of ensembles unwieldy in a particular order (e.g. A^*-A^* ensembles in the zeroth order). Conditional probabilities are truncated to order n by only retaining *conditioning* sites (e.g. α^*) within n lattice vectors of the *conditioned* site (e.g. A^*). Therefore, the zeroth-order truncation in Scheme 4(b) is rigorously derived as

$$\theta_{A^*-A^*} = \chi_{A^*-\alpha^*} \times \theta_{A^*} \xrightarrow{\substack{0^{th}\ order \\ truncation}} \chi_{A^*} \times \theta_{A^*} = \theta_{A^*} \times \theta_{A^*} \qquad \textbf{[16]}$$

where the zeroth order truncates $\chi_{A^*-\alpha^*}$ to $\chi_{A^*} = \theta_{A^*}$ because A^* and α^* are separated by more than zero lattice vectors. Similarly, the first order truncation in Scheme 4(b) is

$$\theta_{A^*-A^*-A^*} = \chi_{A^*-\alpha^*-\alpha^*} \times \theta_{A^*-A^*} \xrightarrow{\substack{1^{st}\ order \\ truncation}} \chi_{A^*-\alpha^*} \times \theta_{A^*-A^*} = \frac{\theta_{A^*-A^*}}{\theta_{A^*}} \times \theta_{A^*-A^*} \qquad \textbf{[17]}$$

where the first order truncates $\chi_{A^*-\alpha^*-\alpha^*}$ to $\chi_{A^*-\alpha^*} = \theta_{A^*-A^*}/\theta_{A^*}$ because A^* and the rightmost α^* are separated by more than one lattice vector. Ensemble-specific rate equations used in the Case Studies to follow are derived by (i) enumerating relevant ensembles as in Scheme 3 and Eq. **14** and (ii) truncating unwieldy ensembles by the procedure exemplified in Eqs. **16** and **17**. For example, Eq. **14** is truncated to the first order by re-writing in terms of conditional probabilities

$$r_{sr[A^*-A^*]} = -k_{sr}\theta_{A^*-A^*}\left[1 + 2\chi_{A^*-\alpha^*-\alpha^*} + 4\chi_{\substack{A^*-\alpha^* \\ | \\ \alpha^*}}\right] \qquad \textbf{[18]}$$

and truncating as in Eq. **17** to give

$$r_{sr[A^*-A^*]} = -k_{sr}\theta_{A^*-A^*}[1 + 2\chi_{A^*-\alpha^*} + 4\chi_{A^*-\alpha^*}] = k_{sr}\theta_{A^*-A^*} \times \left[-1 - 6\frac{\theta_{A^*-A^*}}{\theta_{A^*}}\right] \qquad \textbf{[19]}$$

The bracketed term is the ensemble-specific stoichiometric coefficient $\nu_{sr,[A^*-A^*]}$ and is reported in Table 2 and visualized in Scheme 5. Ensemble-specific elementary step rates are, in general, a product of the fundamental rate of the step (e.g. $k_{sr}\theta_{A^*-A^*}$) and the ensemble-specific stoichiometric coefficient (e.g. $\nu_{sr,[A^*-A^*]} = -[1 + 6\theta_{A^*-A^*}/\theta_{A^*}]$). Our recent work [12] derives and tabulates ensemble-specific first-order rate equations for all one- and two-site elementary steps including surface diffusion (e.g. $A^* + * \rightleftharpoons * + A^*$). Rigorous incorporation of lateral adsorbate interactions into ensemble-specific elementary step rates is detailed in Section 4.2 and, more thoroughly, in our recent work [12].

2.2 Definition of kinetic descriptors

We assess the kinetic descriptions of the Langmuir-Hinshelwood, first order, second order, and kMC methods by comparison of reactions orders, degrees of rate control, and degrees of selectivity control – all of which we calculate from reaction sensitivities, the salient descriptor of composite reactions [26–33].

The sensitivity of step *i* is the fractional change in turnover rate, *r*, per fractional change in rate constant k_i

$$s_i = \left(\frac{\partial \ln r}{\partial \ln k_i}\right)_{k_{j\neq i}} \quad \textbf{[20]}$$

The reaction order of a fluid phase species *j*, Ψ_j, quantifies the increment ($\Psi_j > 0$) or decrement ($\Psi_j < 0$) in rate achieved by increase of thermodynamic activity of species *j*, a_j, and is related to reaction sensitivities by

$$\Psi_j \equiv \left(\frac{\partial \ln r}{\partial \ln a_j}\right)_{a_{k\neq j}} = -\sum_{i=steps} s_i \nu_{ij} [\nu_{ij} < 0] \quad \textbf{[21]}$$

where brackets in Eq. **21** are per Iverson Bracket notation, ν_{ij} is the stoichiometric coefficient of fluid phase species *j* in step *i*, and $[\nu_{ij} < 0]$ is unity if the enclosed inequality is true and zero if false [26,27].

The sum of the forward and reverse sensitivity of step *i* is the kinetic degree of rate control, $X_{RC,i}$, of the shared transition state, *TS,i*, given by

$$s_i + s_{-i} = X_{RC,i} = \left(\frac{\partial \ln r}{\partial(-G^0_{TS,i}/k_B T)}\right)_{G^0_{j\neq TS,i}} = \left(\frac{\partial \ln r}{\partial \ln k_i}\right)_{k_{j\neq i}, K_i} \quad \textbf{[22]}$$

where $-G^0_{TS,i}$ is the standard free energy of the transition state in step *i*. Degrees of rate control are constrained by the condition

$$\sum_{i=steps} X_{RC,i} = 1 \quad \textbf{[23]}$$

for each overall reaction. If there exists a single rate-determining step (rds), $X_{RC,rds} = 1$ and $X_{RC,i\neq rds} = 0$. In branched reaction networks, the degree of selectivity control is defined in terms of the selectivity, *S*, of a specified product

$$X_{SC,i} = \left(\frac{\partial \ln S}{\partial \ln k_i}\right)_{k_{j\neq i}, K_i} \quad \textbf{[24]}$$

which is subject to the constraint $\Sigma_i X_{SC,i} = 0$ and, analogously to $X_{RC,i}$, is a sum of reaction *selectivity* sensitivities

$$X_{SC,i} = s_{Sel,i} + s_{Sel,-i} = \left(\frac{\partial \ln S}{\partial \ln k_i}\right)_{k_{j\neq i}} + \left(\frac{\partial \ln S}{\partial \ln k_{-i}}\right)_{k_{j\neq -i}} \quad \textbf{[25]}$$

Reaction/selectivity sensitivities and degrees of rate/selectivity control defined in Eqs. **20**, **21** – **25** are calculated from partial derivative of the rate or selectivity function with respect to elementary step rate constants at a given temperature and concentration(s); however, as Scheme 2 demonstrates, there is not a single rate – or, by extension, rate constant – assignable to each elementary step. Rather, each elementary step is described by a set of ensemble-specific rates which, for truncation orders greater than zero, are functionally distinct (i.e. depend on distinct ensemble coverages). Distinct ensemble-specific rates for each step i and ensemble j, $r_{i,[j]}$, are attended by distinct rate constants, $k_{i,[j]}$, and, therefore, distinct reaction sensitivity, $s_{i,[j]}$. Zeroth-order, or Langmuir-Hinshelwood, formalisms are ignorant to distinct ensemble-specific elementary step descriptors because consideration solely of single-site coverages effects ensemble-specific rates which are all functionally-equivalent and vary only by numeric stoichiometric coefficients. In higher-order formalisms, $s_{i,[j]}$ carry profound information regarding the kinetic influence of each ensemble; and, as we reported [12], sum to yield conventional reaction sensitivity defined in Eq. **20**

$$s_i = \sum_{\substack{j=independent \\ site\ ensembles}} s_{i,[j]} = \sum_j \left(\frac{\partial \ln r}{\partial \ln k_{i,[j]}}\right)_{k_{m,[n]\neq i,[j]}} \quad \textbf{[26]}$$

where *j* is an index over all independent site ensembles (i.e. those ensembles not relatable by site balances). Ensemble-specificity of reaction sensitivities confers ensemble-specificity of degrees of rate control

$$X_{RC,i} = \sum_j X_{RC,i,[j]} = \sum_j \left(\frac{\partial \ln r}{\partial \ln k_{i,[j]}} \right)_{k_{m,[n]\neq i,[j]}, K_{i,[j]}} \quad \textbf{[27]}$$

and degrees of selectivity control

$$X_{SC,i} = \sum_j X_{SC,i,[j]} = \sum_j \left(\frac{\partial \ln S}{\partial \ln k_{i,[j]}} \right)_{k_{m,[n]\neq i,[j]}, K_{i,[j]}} \quad \textbf{[28]}$$

If, for a given step, there exists a rate-determining ensemble (rde), then $X_{RC,i,[rde]} = X_{RC,i}$ and $X_{RC,i,[j\neq rde]} = 0$. Similarly, an ensemble, *sde*, is considered entirely responsible for the selectivity-control of a step if $X_{SC,i,[sde]} = X_{SC,i}$ and $X_{SC,i,[j\neq sde]} = 0$. In Case Study I to follow, ensemble-specific degrees of selectivity control, $X_{SC,i,[j]}$, will prove virtuous in explicating the inaccuracies of the Langmuir-Hinshelwood formalism and identifying the ensembles which prescribe selectivity between catalytic paths proceeding through ensembles of disparate size.

2.3 Kinetic Monte Carlo Simulation

Lattice-based kinetic Monte Carlo (kMC) simulation provides an exact stochastic-computational description of catalytic surface reactions under any specified conditions (e.g. Conditions (I)-(III)) and, therefore, serves as a useful reference by which to evaluate accuracy of the higher-order kinetic formalism detailed herein. As results to follow demonstrate, the higher-order formalism agrees quantitatively with all kMC-calculated kinetic descriptors at far less computational expense. We posit that, so long as the truncation order is sufficiently large (≈ size of largest reactive ensemble – 1), higher-order formalisms will concur with kMC simulation and provide physical information inaccessible to the non-analytical technique (e.g. ensemble-specific degrees of rate and selectivity control). We note that both kMC and higher-order methods are

robust to inclusion of energetic adsorbate interactions and suggest kMC simulation may be preferred if required truncation orders are prohibitively large (e.g. $\gtrsim$4) and consequent unwieldy microkinetic models. The difficulties presented by magnitude of $\gtrsim$4-order microkinetic models may be overcome by efficient computational-algorithmic generation of rate equations – a challenge we encourage readers to pursue.

We perform kMC simulation on square lattices of size $>128^2$ with periodic boundary conditions. In each iteration, the kMC algorithm selects, at random, an elementary step i to execute with probability p_i correspondent to elementary step rates determined by the law of mass action (e.g. $p_{sr} = k_{sr}\theta_{A*-A*}\,[\Sigma_j\, r_j]^{-1}$). The selected step is performed on an appropriate ensemble chosen at random, the lattice is updated, and the algorithm iterates. In this manner, the lattice-based kMC method is able to simulate catalytic reaction sequences with complete retention of spatial information. Provided the lattice is sufficiently large, populations of ensembles of arbitrary size, shape, and composition are exactly calculable by the square-lattice kMC algorithm.

After each Monte Carlo event, Poisson time is incremented by

$$\delta t \;=\; \frac{-\ln(\rho)}{\sum_j r_j} \qquad \textbf{[29]}$$

where the denominator is a sum over the rates of all elementary step processes and ρ is a uniformly-distributed random number between zero and unity. Poisson time is used to calculate steady-state overall and ensemble-specific elementary step rates for quantitative comparison to analytical kinetic descriptions.

Matlab code used to perform kinetic Monte Carlo simulations in this work may be found at the link https://github.com/neilrazdan/RazdanBhan-SiteEnsembles or by communication with the authors.

3. Results

…

We explicate the limitations and inaccuracies of the Langmuir-Hinshelwood formalism by comparison with first-order, second-order, and lattice-based kMC descriptions in the context of three conceptually-distinct case studies. Case Studies I-III respectively demonstrate that the Langmuir-Hinshelwood formalism (I) is unable to account for the propensity of multi-site ensembles to dictate selectivity, (II) cannot reliably calculate elementary step activation entropies and enthalpies, and (III) is incorrect even in the limit of infinitely-fast surface diffusion if adsorbates occupy more than one site (e.g. ${}^{*}C_nH_m{}^{*}$ in catalytic alkane hydrogenolysis [18]).

3.1 Case Study I: $A + A \rightarrow A_2$ with competitive Eley-Rideal pathway $A + B \rightarrow AB$

The catalytic consequences of distinct ensemble site requirements on selectivity has been proposed as an important consideration in competitive alkane (de-)hydrogenation and hydrogenolysis [4,34,35], olefin epoxidation and combustion [1,2,36], and hydrodeoxygenation and hydrogenolysis [37,38]. We examine the profundity of ensemble clustering/isolation in determining selectivity by comparing zeroth-order, first-order, and kMC description of competitive scavenging of immobile, thermodynamically-ideal adsorbed A^* species via (i) two-site surface reaction A^*–$A^* \rightarrow A_{2(g)}$ + *–* and (ii) one-site Eley-Rideal reaction $A^* + B_{(g)} \rightarrow AB_{(g)}$ + * (Table 1).

Table 1: Bimolecular catalytic reaction with competitive Eley-Rideal pathway

#	Step	Rate constants
1	$A_{(g)} + * \rightarrow A^*$	$k_{ads} = 1$ (bar · s)$^{-1}$
–1	$A^* \rightarrow A_{(g)} + *$	$k_{des} = 1$ s^{-1}
2	$A^* - A^* \rightarrow A_{2(g)} + * - *$	$k_{sr} = 50$ s^{-1}
3	$B_{(g)} + A^* \rightarrow AB_{(g)} + *$	$k_{ER} = 1$ (bar · s)$^{-1}$

We note Case Study I is an extension of an example presented in our recent work [12] which studies the $2A_{(g)} \rightarrow A_{2(g)}$ reaction described by steps 1, –1, and 2 in Table 1 to explicate the capacity of the first-order and kMC descriptions to correctly account for A^*–A^* partitioning (i.e. $\theta_{A*-A*} << \theta_{A*}^2$) and identify $A_{(g)}$ sorption is *both equilibrated and rate-determining* – an apparent impossibility per the Langmuir-Hinshelwood formalism. The ostensible paradox of an equilibrated, rate-determining step is resolved by examination of ensemble-specific elementary step rates which reveal $A_{(g)}$ sorption is equilibrated in the sense $r_{des}/r_{ads} = 1$, but is irreversible with respect to scarce A^*–A^* pairs unperturbed by desorption of stranded A^* (i.e. $r_{des,[A*-A*]}/r_{ads,[A*-A*]} = 0$). We therefore surmise that $A_{(g)}$ sorption is not *entirely* equilibrated, permitting the step to be rate-determining and equilibrated in the canonical sense (i.e. $r_{des}/r_{ads} = 1$) [12].

The reaction sequence in Table 1 is described by the zeroth-order and first-order formalisms by respective one-site and ≤two-site ensemble-specific elementary-step rates reported in Table 2. The ensemble-specific rate of each elementary step is the product of (i) the fundamental rate of the step (e.g. $r_{des} = k_{des}\theta_{A*}$ for $A_{(g)}$ desorption) and (ii) the appropriate ensemble-specific stoichiometric coefficient (e.g. $\nu_{des,[A*-A*]} = -2\theta_{A*-A*}/\theta_{A*}$ in the first order) – as is illustrated in Scheme 5. The Hinshelwood approximation prohibits identification of two-site ensemble-specific stoichiometric coefficients; and, therefore, the Langmuir-Hinshelwood formalism contains no such entries in Table 2. Instead, the full zeroth-order microkinetic model only explicitly describes dynamics of single-site ensembles A^* and * by (i) use of overall site balance $\theta_* = 1 - \theta_{A*}$ and (ii) forward integration of rate equation for A^* species

$$\frac{d\theta_{A^*}}{dt} = k_{ads}P_A\theta_* - k_{des}\theta_{A^*} - 4k_{sr}\theta_{A^*}^2 - k_{ER}P_B\theta_{A^*} \qquad \textbf{[30]}$$

determined by use of grey-shaded entries in Table 2.

Table 2: Elementary step rates in the Langmuir-Hinshelwood and first-order formalisms

	Langmuir-Hinshelwood				First-order			
Step, i	*ads.*	*des.*	*rxn.*	*E-.R.*	*adsorption*	*desorption*	*reaction*	*Eley-Rideal*
Rate, r_i	$k_{ads}P_A\theta_*$	$k_{des}\theta_{A^*}$	$k_{sr}\theta_{A^*}^2$	$k_{ER}P_B\theta_{A^*}$	$k_{ads}P_A\theta_*$	$k_{des}\theta_{A^*}$	$k_{sr}\theta_{A^*-A^*}$	$k_{ER}P_B\theta_{A^*}$
***Ensemble-Specific Stoichiometric Coefficients*, $\nu_{i,[j]}$**								
$\nu_{i,[A^*]}$	1	– 1	– 4	– 1	1	– 1	– 4	– 1
$\nu_{i,[*]}$	– 1	1	4	1	– 1	1	4	1
$\nu_{i,[A^*-A^*]}$	No explicit rate equations. $\theta_{ij} = \theta_i\theta_j$				$\frac{2\theta_{A^*-*}}{\theta_*}$	$-\frac{2\theta_{A^*-A^*}}{\theta_{A^*}}$	$-1-\frac{6\theta_{A^*-A^*}}{\theta_{A^*}}$	$-\frac{2\theta_{A^*-A^*}}{\theta_{A^*}}$
$\nu_{i,[A^*-*]}$					$\frac{\theta_{*-*}-\theta_{A^*-*}}{\theta_*}$	$\frac{\theta_{A^*-A^*}-\theta_{A^*-*}}{\theta_{A^*}}$	$\frac{3(\theta_{A^*-A^*}-\theta_{A^*-*})}{\theta_{A^*}}$	$\frac{\theta_{A^*-A^*}-\theta_{A^*-*}}{\theta_{A^*}}$
$\nu_{i,[*-*]}$					$-\frac{2\theta_{*-*}}{\theta_*}$	$\frac{2\theta_{A^*-*}}{\theta_{A^*}}$	$1+\frac{6\theta_{A^*-*}}{\theta_{A^*}}$	$\frac{2\theta_{A^*-*}}{\theta_{A^*}}$
***Ensemble-Specific Elementary Step Rates*, $r_{i,[j]}$**								
$r_{i,[j]} = r_i \times \nu_{i,[j]}$								

The rate equation for an elementary step with respect to a particular site ensemble is the product of (i) the fundamental rate of the step in the row labeled 'Rate, r_i' and (ii) the ensemble-specific stoichiometric coefficient of the concerned ensemble. For example, in the first order, $r_{ER,[A^*-A^*]} = r_{ER} \times \nu_{ER,[A^*-A^*]} = k_{ER}P_B\theta_{A^*} \times (-2\theta_{A^*-A^*}/\theta_{A^*})$. Grey-shaded, blue-shaded, and pink-shaded entries respectively are used for derivation of Eqs. **30**, **31**, and **32**. The blue-shaded entries are also visually derived in Scheme 5. First-order ensemble-specific stoichiometric coefficients for adsorption and desorption were derived in Eqs. **5 – 7** and illustrated in Scheme 2.

Scheme 5: Visualization of Eq. **31** and blue-shaded entries of **Table 2**†

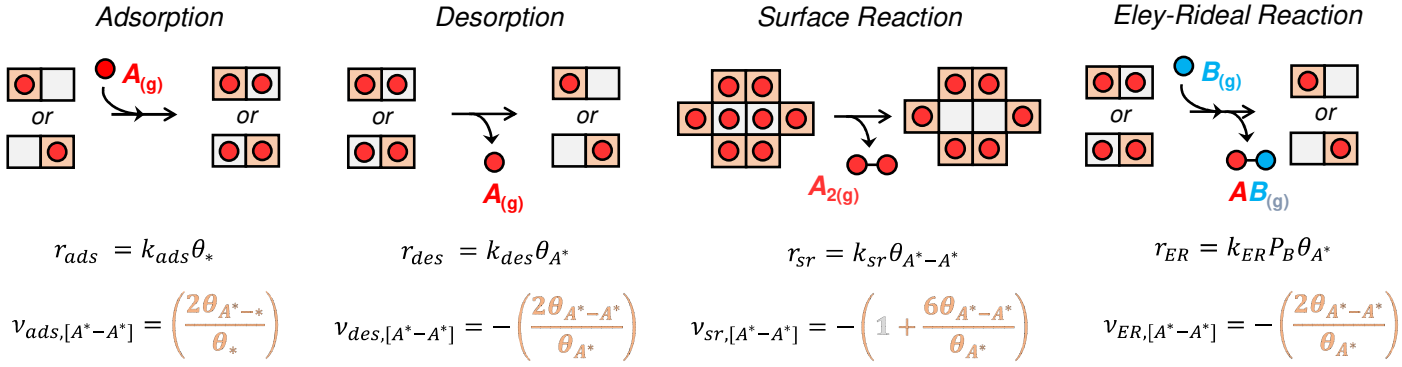

†Visualization of [A^*–A^*]-specific rates reported in blue-shaded entries of Table 2 and in Eq. **31**. The rate of each elementary step with respect to A^*–A^* pairs is illustrated with white-colored sites (□) hosting the elementary step and orange-colored sites (□) spatially coupling to generate/consume A^*–A^* pairs. The number of □-sites in illustration of each step corresponds to the numeric factor adjoining each ensemble-specific stoichiometric coefficient. For example, there are six □-sites neighboring the □□ pair hosting surface reaction and, correspondingly, the stoichiometric coefficient $\nu_{r,[A^*-A^*]}$ contains a factor of '6'. The additional additive factor of unity accounts for the necessary reactive A^*–A^* pair and is thusly shaded white rather than orange.

The first-order formalism wholly describes the dynamics of five ensembles {*, A^*, *–*, A^*–*, A^*–A^*}, coverages of which are constrained by one overall ($1 = \theta_* + \theta_{A^*}$) and two component ($\theta_j$

$= \theta_{j-*} + \theta_{j-A^*}$ for $j = *, A^*$) site balances. The full first-order microkinetic model therefore requires $5 - 3 = 2$ rate equations

$$\frac{d\theta_{A^*-A^*}}{dt} = 2k_{ads}P_A\theta_{A^*-*} - 2k_{des}\theta_{A^*-A^*} - k_{sr}\theta_{A^*-A^*}\left(1 + 6\frac{\theta_{A^*-A^*}}{\theta_{A^*}}\right) - 2k_{ER}P_B\theta_{A^*-A^*} \quad \textbf{[31]}$$

and

$$\frac{d\theta_{A^*-*}}{dt} = k_{ads}P_A(\theta_{*-*} - \theta_{A^*-*}) + k_{des}(\theta_{A^*-A^*} - \theta_{A^*-*}) + k_{sr}\theta_{A^*-A^*}\frac{3(\theta_{A^*-A^*} - \theta_{A^*-*})}{\theta_{A^*}} + k_{ER}P_B(\theta_{A^*-A^*} - \theta_{A^*-*}) \quad \textbf{[32]}$$

respectively determined by use of blue- and pink-shaded entries in Table 2. Eqs. **31** and **32** exemplify the ensemble-specificity of the first-order formalism and kinetically describe the unique reaction paths experienced by each ensemble. For example, Scheme 5 illustrates the [A^*–A^*]-specific path described by Eq. **31** to aid visualization of the ensemble-specific spatial coupling responsible for each coverage-dependent stoichiometric coefficient $\nu_{i,[A^*-A^*]}$ for steps $i = \{ads, des, sr, ER\}$. As Scheme 5 depicts, surface reaction is capable of eliminating as many as seven A^*–A^* pairs per elementary step event (i.e. $[1 + 6\theta_{A^*-A^*}/\theta_{A^*}]_{max} = 7$) and, thusly, strands self-annihilating A^* species if $k_{sr} >> k_{i\neq sr}$ – as is the case per Table 1. Results to follow demonstrate that seclusion of A^* species unidentifiable in the Langmuir-Hinshelwood formalism is quantitatively accounted for by the first-order and kMC methods and manifests in preponderance of A^*–* pairs which selectively promote one-site Eley-Rideal reaction indifferent to the scarcity of A^*–A^*.

Preparatory to examination of Figs. 1 – 3, we encourage readers to replicate the ensemble-specific stoichiometric coefficients in Table 2 by construction and inspection of visual aids akin to Schemes 2, 3, and 5. Interpretation of results hereinafter is predicated on physical meaning and mathematical provenance of first-order rate terms derived hereinbefore.

Figure 1 shows coverages, selectivities, and mean-field metrics of the reaction system in Table 1 calculated by the Langmuir-Hinshelwood (LH), first-order, and kMC methods. First-order- and kMC-calculated descriptors quantitatively agree for $P_A = 10^{-3}$ –10^{3} bar and all three models are in agreement for $P_A > 10$ bar; high $A_{(g)}$ pressures beget an A^*-covered surface (Fig. 1(A)), giving $\theta_{A^*-A^*} = \theta_{A^*} = \mu_{A^*-A^*} = 1$ (Fig. 1(C)) and 100% selectivity to $A_{2(g)}$ formation which benefits from high A^* coverages more profoundly than $AB_{(g)}$ formation (Fig. 1(B)).

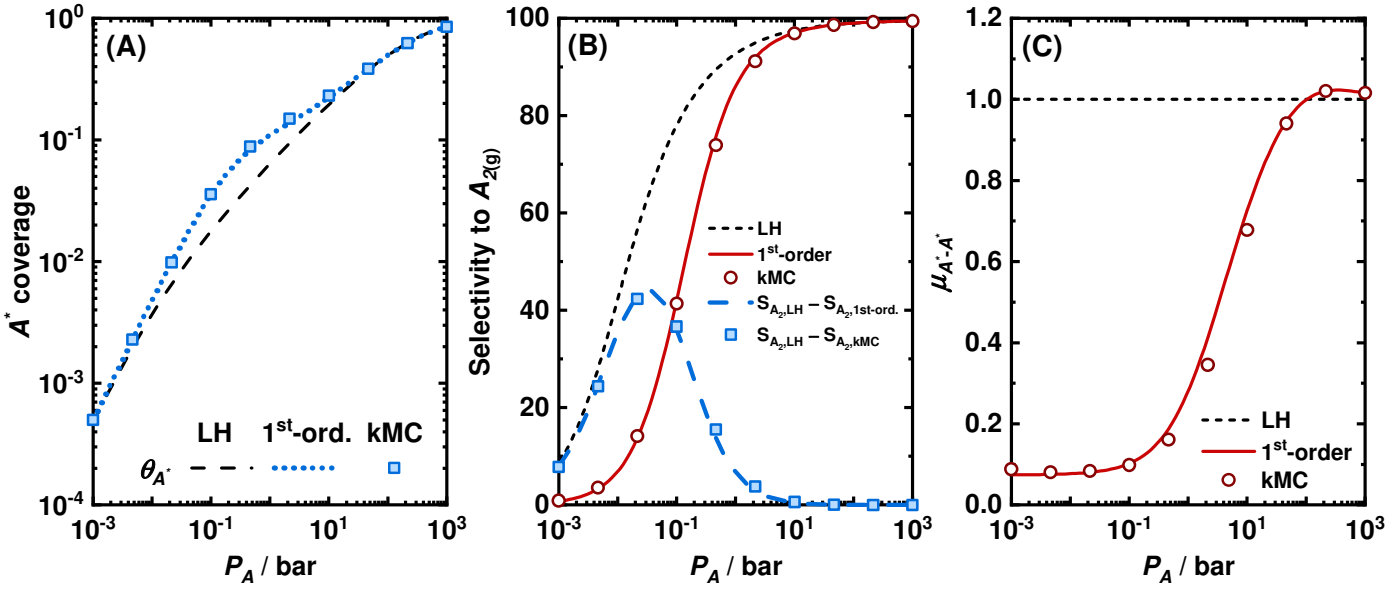

Fig. 1: (A) Fractional coverage $\theta_{A^*} = R_{AB}(P_B k_{ER})^{-1}$ calculated by the Langmuir-Hinshelwood (– –), first-order (···), and kMC (□) methods. (B) Selectivity to $A_{2(g)}$ calculated by model j, $S_{A_2,j}$, calculated by the Langmuir-Hinshelwood (- - -), first-order (—), and kMC (○) methods. Differences in calculated selectivities $S_{A_2,LH} - S_{A_2,1^{st}\text{-}ord.}$ (– –) and $S_{A_2,LH} - S_{A_2,kMC}$ (□). (C) Mean-field metric $\mu_{A^*-A^*}$ calculated by the Langmuir-Hinshelwood (- - -), first-order (—), and kMC (○) methods. Calculations are of the reaction network in Table 1 with $P_B = 1$ bar. Standard mean error bars for kMC simulation are smaller than corresponding symbols and are therefore not shown.

Pressures of $A_{(g)}$ below 10 bar effect significant isolation of A^* species quantified by $\mu_{A^*-A^*} << 1$ with asymptotic approach of $\mu_{A^*-A^*} \rightarrow 0.1$ for $P_A \rightarrow 0$ (Fig. 1(C)). In the same regime for which the Langmuir-Hinshelwood model overestimates $\theta_{A^*-A^*}$ by ≤10×, A^* coverage is underestimated by as much as ~5× (Fig. 1(A); $P_A = 10^{-2}$ –10^{1} bar). Although ostensibly antithetical, respective

over- and under-prediction of $\theta_{A^*-A^*}$ and θ_{A^*} by the zeroth-order formalism both result from k_{sr} >> $k_{i\neq sr}$ which effects rapid annihilation of A^*–A^* pairs, thereby engendering isolation (i.e. $\mu_{A^*-A^*}$ << 1) and accumulation (i.e. increment in θ_{A^*}) of A^* species due to the scarcity of A^* neighbors with which to react. As discussed heretofore and quantified by the mean-field metric balance in Eq. **11**, the segregation of A^*–A^* is necessarily attended by an accumulation of A^*–* pairs selective for the one-site Eley-Rideal reaction. Consequently, $A_{2(g)}$ selectivities are decremented relative to a uniform surface and are overestimated by the Langmuir-Hinshelwood model by as much as 45% (Fig. 1(B)). The inability of the zeroth-order formalism to capture isolation of A^* species prohibits quantitative description of selectivity-control exercised by the A^*–A^* and A^*–* ensembles which (i) necessarily aggregate and segregate in concert (Eq. **11**) and (ii) promote distinct reaction paths.

Figure 2 compares degrees of selectivity control calculated by the zeroth-order, first-order, and kMC methods to guide interpretation of pertinent kinetic information overlooked by the Hinshelwood approximation. $X_{SC,i}$ calculated by all three models converge to zero for large P_A because A^*-saturation of the surface attenuates selectivity control of all steps. Low $A_{(g)}$ pressures bare the surface (Fig. 1(A)), effecting asymptotic approach of all $X_{SC,i}$ as $P_A \rightarrow 0$. On bare surfaces, one-site $A_{(g)}$ sorption and Eley-Rideal steps respectively promote and suppress $A_{2(g)}$ selectivity in both the zeroth and first order formalisms because of respective propensities of each step to generate and scavenge A^*–A^* pairs. The Langmuir-Hinshelwood formalism incorrectly identifies surface reaction as selectivity-determining ($X_{SC,sr}$ = 1) because of the miscalculated abundance of reactive A^*–A^* ensembles; in actuality, increase to k_{sr} exacerbates 'transport-limitations' which strand A^* and render surface reaction ineffective in improving selectivity ($X_{SC,sr}$ ~ 0).

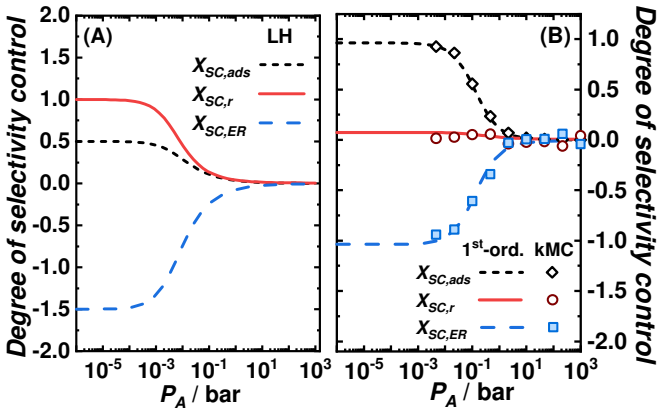

Fig. 2: Degrees of selectivity control calculated by (A) the Langmuir-Hinshelwood formalism and (B) the first-order formalism and kMC method. Calculations are of the reaction network in Table 1 with P_B = 1 bar. Standard mean error bars for kMC simulation are smaller than corresponding symbols and are therefore not shown. X_{SC} are not calculated by the kMC method for $P_A \leq 10^{-3}$ because A^* coverages are prohibitively small for numerical differentiation.

The decrement in $X_{SC,sr}$ relative to a uniform surface is re-apportioned to increase in $X_{SC,ads}$ and $X_{SC,ER}$. The dearth of A^*–A^* pairs reinforces the kinetic burden on $A_{(g)}$ adsorption to generate reactive pairs and consequents $X_{SC,ads} = -X_{SC,ER} = 1$ from which we surmise the selectivity to $A_{2(g)}$ is entirely controlled by the competition between (i) adsorption which adjoins A^*–* ensembles with $A_{(g)}$ to create A^*–A^* pairs and (ii) Eley-Rideal reaction which scavenges A^*–* ensembles with $B_{(g)}$ to create $AB_{(g)}$. We quantitatively assess this interpretation and the contribution of A^*–* and A^*–A^* ensembles to the selectivity control of each step by calculation of ensemble-specific $X_{SC,i,[j]}$ only identifiable in higher-order, analytical formalisms.

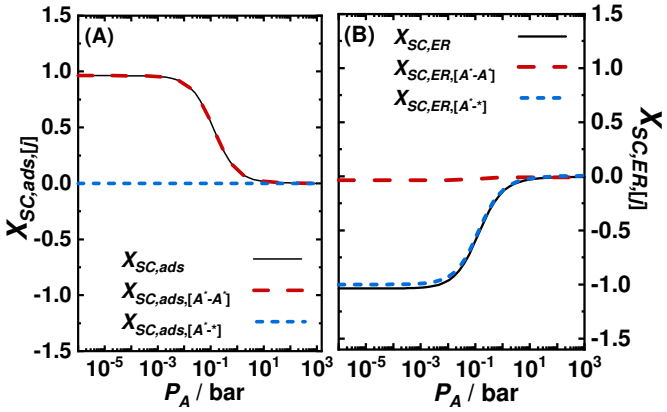

Fig. 3: Ensemble-specific degrees of selectivity control for (A) adsorption of $A_{(g)}$ and (B) Eley-Rideal reaction. Calculations are of the reaction network in Table 1 with P_B = 1 bar. Ensemble-specific $k_{i,[j]}$ are not definable in the kMC method and, therefore, $X_{SC,i,[j]}$ cannot be calculated.

Figures 3(A) and 3(B) respectively show $X_{SC,ads,[j]}$ and $X_{SC,ER,[j]}$ for j = {A^*–*, A^*–A^*} calculated from application of Eq. **28** to the first-order microkinetic model, Eqs. **31**-**32**. Selectivity control of $A_{(g)}$ sorption and Eley-Rideal reaction are respectively entirely attributable to the creation of A^*–A^* ensembles and scavenging of A^*–* ensembles – evincing interpretation of $X_{SC,i}$ in Fig. **2**. The elementary adsorption step ($A_{(g)}$ + A^*–* ⇌ A^*–A^*) occurs with rate $r_{ads,[A^*-A^*]} = 2k_{ads}P_A\theta_{A^*-*} - 2k_{des}\theta_{A^*-A^*} \approx 2k_{ads}P_A\theta_{A^*-*}$, as illustrated in Scheme 2, and is the only process capable of generating the requisite, rapidly self-annihilating A^*–A^* pairs. This kinetic burden on $A_{(g)}$ sorption to create exiguous A^*–A^* pairs is manifest in $X_{SC,ads} = X_{SC,ads,[A^*-A^*]} = 1$. The [$A^*$–*]-specific selectivity control of sorption is negligible because A^*–* constitute ≥97% of A^*–j pairs and are already produced by the majority of adsorption events since $\theta_{*-*} >> \theta_{A^*-*}$.

The preponderance of A^*–* is, however, largely responsible for the selectivity control of Eley-Rideal reaction. $AB_{(g)}$ formation occurs with rate $r_{ER} = k_{ER}P_B(\theta_{A^*-*} + \theta_{A^*-A^*}) \approx k_{ER}P_B\theta_{A^*-*}$ and is therefore most accelerated by A^*–* ensembles which outnumber A^*–A^* by ~10^4×. Accordingly, $|X_{SC,ER,[A^*-*]}| >> |X_{SC,ER,[A^*-A^*]}|$ and $X_{SC,ER,[A^*-*]} \approx X_{SC,ER}$. The ensemble-specificity of compendious kinetic descriptors such as $X_{SC,ER,[A^*-*]}$ are incalculable in the zeroth-order

formalism or kMC method and quantitatively inform interpretation of ensemble site effects observed to dictate selectivity in catalytic reactions of industrial interest [1,2,35,36]. We postulate that the limitations of the Hinshelwood approximation, bared herein, grow in significance with the size of elementary step ensembles and, therefore, particularly caution against the use of the Langmuir-Hinshelwood formalism for reactions proceeding through large catalytic site ensembles.

In the following example, we further explicate the unreliability of the Langmuir-Hinshelwood formalism for description of multi-site catalytic sequences by comparing intrinsic elementary step activation barriers calculated using zeroth- and first-order closed-form rate expressions.

3.2 Case Study II: Activation parameters of rate-determining steps in A + ½B₂ → AB

Chemical interpretation of rate-determining steps/transition states in catalytic reaction sequences is predicated on the determination of elementary step activation enthalpies, $\Delta H_{rds}^{0,\ddagger}$, and entropies, $\Delta S_{rds}^{0,\ddagger}$, to discern quantitative, molecular-level insight concerning the interactions which dictate reactivity. Calculation of $\Delta H_{rds}^{0,\ddagger}$ and $\Delta S_{rds}^{0,\ddagger}$ relies on fitting experimentally-measured kinetic data with mechanistically-based rate expressions which, to-date, have almost exclusively been derived using the Langmuir-Hinshelwood formalism. Examples include kinetic studies of catalytic alkane hydrogenolysis and dehydrogenation [4,6–8,34], aldol condensation [39], methanol oxidative dehydrogenation [40], water gas shift [26,28], formic acid dehydrogenation [5], and methane reforming and oxidation [41,42] – all of which proceed through rate-determining steps occurring on two sites (e.g. rate-determining $CH_{4(g)} + *\text{–}O^{*} \rightarrow CH_3{}^{*}\text{–}OH^{*}$ in methane reforming). As we demonstrated previously [12] and explicate again herein, the Langmuir-Hinshelwood formalism cannot explicitly enumerate populations of two-site reactive

ensembles (e.g. *–O^* required to activate methane) and is therefore unreliable for identification of rate-determining steps and/or elementary step activation parameters – even if Langmuir-Hinshelwood rate expressions describe measured rate data quantitatively.

Table 3: Elementary steps and activation parameters of bimolecular catalytic surface reaction

#	Step	k_i(300 K)	$\Delta H_i^{0,\ddagger}$ kJ mol^{-1}	$\Delta S_i^{0,\ddagger}$ J mol^{-1} K^{-1}
1	$A_{(g)} + * \rightarrow A^*$	$k_{A,ads}$ = 1 (bar · s)$^{-1}$	36.1	–124.6
–1	$A^* \rightarrow A_{(g)} + *$	$k_{A,des}$ = 10^3 s^{-1}	65.0	29.3
2	$B_{2(g)} + * - * \rightarrow B^* - B^*$	$k_{B_2,ads}$= 1 (bar · s)$^{-1}$	36.1	–124.6
–2	$B^* - B^* \rightarrow B_{2(g)} + * - *$	$k_{B_2,des}$ = ½ · 10^4 s^{-1}	55.4	10.5
3	$A^* - B^* \rightarrow AB_{(g)} + * - *$	k_{sr} = ¼ · 10^5 s^{-1}	45.7	–8.3

Consider the bimolecular catalytic reaction $A + ½B_2 \rightarrow AB$ transpiring through the series of elementary steps in Table 3 wherein all adsorbed species are immobile. Two-site requirements for $B_{2(g)}$ sorption and A^*–B^* surface reaction steps prohibit virtuous use of the Hinshelwood approximation and demand a first-order kinetic description to explicitly enumerate kinetically-relevant site pairs (e.g. *–* pairs required for and eliminated by $B_{2(g)}$ adsorption). Tables 4(A) and 4(B) compare elementary steps rates for select ensembles in the zeroth-order and first-order formalisms, respectively. Ensemble-specific elementary step rates for remaining ensembles {B^*, B^*– B^*, B^*–*, *–*} are tabulated in Section S1.

Table 4(A): Select rate equations in the Langmuir-Hinshelwood (zeroth-order) formalism

	Langmuir-Hinshelwood				
Step, i	$A_{(g)}$ *ads.*	$A_{(g)}$ *des.*	$B_{2(g)}$ *ads.*	$B_{2(g)}$ *des.*	*reaction*
Rate, r_i	$k_{A,ads}P_A\theta_*$	$k_{A,des}\theta_{A^*}$	$k_{B_2,ads}P_{B_2}\theta_*^2$	$k_{B_2,des}\theta_{B^*}^2$	$k_{sr}\theta_{A^*}\theta_{B^*}$
Ensemble-Specific Stoichiometric Coefficients					
$\boldsymbol{\nu_{i,[A^*]}}$	1	– 1	0	0	– 4
$\boldsymbol{\nu_{i,[*]}}$	– 1	1	– 4	4	8
$\boldsymbol{\nu_{i,[A^*-A^*]}}$	No explicit rate equations. $\theta_{ij} = \theta_i\theta_j$				
$\boldsymbol{\nu_{i,[A^*-*]}}$					
$\boldsymbol{\nu_{i,[A^*-B^*]}}$					

The rate equation for an elementary step with respect to a particular site ensemble is the product of (i) the fundamental rate of the step in the row labeled 'Rate, r_i' and (ii) the ensemble-specific stoichiometric coefficient of the concerned ensemble. For example, $r_{A,ads,[A^*]} = r_{A,ads} \times \nu_{A,ads,[A^*]} = k_{A,ads}P_A\theta_* \times 1$.

Table 4(B): Select rate equations in the first-order formalism

	First-order				
Step, i	$A_{(g)}$ *ads.*	$A_{(g)}$ *des.*	$B_{2(g)}$ *ads.*	$B_{2(g)}$ *des.*	*reaction*
Rate, r_i	$k_{A,ads}P_A\theta_*$	$k_{A,des}\theta_{A^*}$	$k_{B_2,ads}P_{B_2}\theta_{*-*}$	$k_{B_2,des}\theta_{B^*-B^*}$	$k_{sr}\theta_{A^*-B^*}$
Ensemble-Specific Stoichiometric Coefficients					
$\boldsymbol{\nu_{i,[A^*]}}$	1	– 1	0	0	– 4
$\boldsymbol{\nu_{i,[*]}}$	– 1	1	– 4	4	8
$\boldsymbol{\nu_{i,[A^*-A^*]}}$	$\frac{2\theta_{A^*-*}}{\theta_*}$	$-\frac{2\theta_{A^*-A^*}}{\theta_{A^*}}$	0	0	$-\frac{6\theta_{A^*-A^*}}{\theta_{A^*}}$
$\boldsymbol{\nu_{i,[A^*-*]}}$	$\frac{\theta_{*-*}-\theta_{A^*-*}}{\theta_*}$	$\frac{\theta_{A^*-A^*}-\theta_{A^*-*}}{\theta_{A^*}}$	$-\frac{3\theta_{A^*-*}}{\theta_*}$	$\frac{3\theta_{A^*-B^*}}{\theta_{B^*}}$	$3\left(\frac{\theta_{A^*-A^*}-\theta_{A^*-*}}{\theta_{A^*}}+\frac{\theta_{A^*-B^*}}{\theta_{B^*}}\right)$
$\boldsymbol{\nu_{i,[A^*-B^*]}}$	$\frac{\theta_{B^*-*}}{\theta_*}$	$-\frac{\theta_{A^*-B^*}}{\theta_{A^*}}$	$\frac{3\theta_{A^*-*}}{\theta_*}$	$-\frac{3\theta_{A^*-B^*}}{\theta_{B^*}}$	$-1-3\left(\frac{\theta_{A^*-B^*}}{\theta_{A^*}}+\frac{\theta_{A^*-B^*}}{\theta_{B^*}}\right)$

The rate equation for an elementary step with respect to a particular site ensemble is the product of (i) the fundamental rate of the step in the row labeled 'Rate, r_i' and (ii) the ensemble-specific stoichiometric coefficient of the concerned ensemble. For example, $r_{A,ads,[A^*-B^*]} = r_{A,ads} \times \nu_{A,ads,[A^*-B^*]} = k_{A,ads}P_A\theta_* \times (\theta_{B^*-*}/\theta_*)$. Grey-shaded entries are used for derivation of Eq. **33**.

From Table 4, we derive zeroth- and first-order closed-form rate expressions for $AB_{(g)}$ formation under conditions

(I) $A_{(g)}$ and $B_{2(g)}$ sorption are equilibrated in the sense $r_{i,des}/r_{i,ads} = 1$

(II) The surface is bare in the sense $\theta_* = 1$, $\theta_{A^*} << 1$, and $\theta_{B^*} << 1$

to explicate zeroth- and first-order calculation of $\Delta H_{rds}^{0,\ddagger}$ and $\Delta S_{rds}^{0,\ddagger}$ from experimental rate data.

Per Condition (I), coverages of A^* and B^* are algebraically-determined by equilibrium constants $K_A \equiv k_{A,ads}/k_{A,des}$ and $K_{B_2} \equiv k_{B_2,ads}/k_{B_2,des}$. Condition (II) further simplifies calculation of A^* and B^* coverages by ensuring adsorption is non-competitive, giving $\theta_{A^*} = K_A P_A$ and $\theta_{B^*} = (K_{B_2} P_{B_2})^{1/2}$. The rate of $AB_{(g)}$ formation per the Langmuir-Hinshelwood formalism is therefore

$$R_{AB_{(g)},LH} = 4k_{sr}\theta_{A^*}\theta_{B^*} = 4k_{sr}K_A P_A \sqrt{K_{B_2} P_{B_2}} \qquad \textbf{[33]}$$

which, with knowledge of K_A and K_{B_2}, is used to determine k_{sr} by fit to experimental rate data which conform with reaction orders $\Psi_A = 1$ and $\Psi_{B_2} = ½$ – as shown in Figure 4.

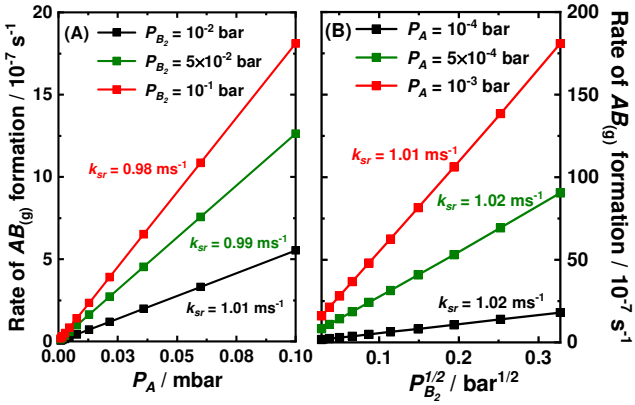

Fig. 4: Rates of $AB_{(g)}$ formation calculated by the full first-order microkinetic model (■) as a function of (A) P_A and (B) $P_{B_2}^{½}$ at 300 K using kinetic parameters in Table 3. 'Rate data' determined by simulation of the full first-order microkinetic model are fit to the closed-form Langmuir-Hinshelwood rate expression in Eq. **33** to calculate $k_{rds} = k_{sr} = 10^3$ s^{-1}. In actuality, *rds* = *A*,*des*, giving $k_{rds} = k_{A,des} = 10^3$ s^{-1} per Eq. **43** and in agreement with Table 3.

Ex situ measurement of sorption equilibrium constants (e.g. by microcalorimetry [43–45] or temperature-programmed desorption [46]), leaves a single unknown kinetic parameter, k_{sr}, determined by linear fit of $R = [4K_A(K_{B_2}P_{B_2})^{1/2}] \times k_{sr}P_A$ and $R = [4K_A P_A K_{B_2}^{1/2}] \times k_{sr}P_{B_2}^{1/2}$ in Figs. 4(A) and 4(B), respectively. Quantitative fits in Fig. 4 calculate $k_{sr} = 10^3$ s^{-1}, underestimating the rate constant of apparently rate-determining surface reaction by 25× (Table 3). Profound miscalculation of k_{sr} is entirely attributed to the erroneous Hinshelwood approximation $\theta_{A^*-B^*} =$

$\theta_{A^*}\theta_{B^*}$ which obfuscates kinetic consequences of A^*–B^* isolation effected by rapid surface reaction. We redress ignorance to A^*–B^* partitioning by derivation of a closed-form, first-order correction to Eq. **33** which clarifies kinetic provenance of the particular combinatorial non-idealities which render the Langmuir-Hinshelwood formalism inappropriate.

The first-order correction to the Langmuir-Hinshelwood rate expression is simply the mean-field metric

$$\mu_{A^*-B^*} \equiv \frac{\theta_{A^*-B^*}}{\theta_{A^*}\theta_{B^*}} = \frac{4k_{sr}\theta_{A^*-B^*}}{4k_{sr}\theta_{A^*}\theta_{B^*}} = \frac{r_{1st}}{r_{LH}} \qquad \textbf{[34]}$$

which we derive in closed form by examination of the steady-state rate equation for A^*–B^* pairs

$$\begin{aligned}\frac{d\theta_{A^*-B^*}}{dt} = 0 = k_{A,ads}P_A\theta_{B^*-*} - k_{A,des}\theta_{A^*-B^*} + 3k_{B_2,ads}P_{B_2}\theta_{*-*}\frac{\theta_{A^*-*}}{\theta_*} \\ - 3k_{B_2,des}\theta_{B^*-B^*}\frac{\theta_{A^*-B^*}}{\theta_{B^*}} - k_{sr}\theta_{A^*-B^*}\left(1 + 3\frac{\theta_{A^*-B^*}}{\theta_{A^*}} + 3\frac{\theta_{A^*-B^*}}{\theta_{B^*}}\right)\end{aligned} \qquad \textbf{[35]}$$

determined by the sum of elementary step rates with respect to A^*–B^* listed in the grey-shaded entries in Table 4(B). Conditions (I) and (II) permit simplification of Eq. **35** by ensuring mean-field metrics for pairs $ij \neq A^*$–B^* are very near unity – as is confirmed and detailed in Section S2.

Briefly, the preponderance of vacant sites and equilibration of sorption ensures all ensembles not dictating rates of disproportionally slow or fast steps are *essentially* randomly-distributed (i.e. $\mu_{ij\neq A^*-B^*}$ deviate negligibly from unity). We emphasize that no mean-field metric is exactly unity; partitioning of A^*–B^* pairs, to be demonstrated in the following, necessarily effects at least one $\mu_{ij\neq A^*-B^*} > 1$ which requires at least one $\mu_{ik\neq A^*-B^*} < 1$ and so on. The near-saturation coverage of vacant sites, however, minimizes requisite deviation from $\mu_{ij\neq A^*-B^*} = 1$ by ensuring weighting factors (θ_*, θ_{A^*}, θ_{B^*}) in the mean-field metric balance (Eq. **11**) are all either unity or very small. Consequently, rapidity of surface reaction effects $\mu_{A^*-B^*} << 1$ without appreciably disturbing combinatorially-ideal distribution of all other ensembles.

Application of Conditions (I) and (II) is therefore useful in re-expressing Eq. **35**

$$\frac{d\theta_{A^*-B^*}}{dt} = 0 = k_{A,ads}P_A\theta_{B^*}\theta_* - k_{A,des}\theta_{A^*-B^*} + 3k_{B_2,ads}P_{B_2}\theta_*^2\theta_{A^*} - 3k_{B_2,des}\theta_{B^*}\theta_{A^*-B^*} - k_{sr}\theta_{A^*-B^*}(1 + 3\mu_{A^*-B^*}\theta_{B^*} + 3\mu_{A^*-B^*}\theta_{A^*}) \quad \textbf{[36]}$$

making use of unity mean-field metrics (i.e. $\mu_{B^*-B^*} = \mu_{B^*-*} = \mu_{*-*} = \mu_{A^*-*} = 1$) to yield quantitatively justifiable zeroth-order coverage terms. We emphasize $\mu_{A^*-B^*}$ cannot reliably be assumed unity because A^*–B^* pairs are the only ensemble dictating the rate of a non-equilibrated elementary step and self-annihilate ≤ 7× per irreversible surface reaction event (i.e. $\nu_{sr,[A^*-B^*]} = [1 + 3\theta_{A^*-B^*}/\theta_{A^*} + 3\theta_{A^*-B^*}/\theta_{B^*}] \leq 7$).

Eq. **36** is simplified by evoking Condition (II) to permit efface of redundant multiplicative and additive identities (i.e. $\theta_* = 1$, $\theta_{A^*} << 1$, and $\theta_{B^*} << 1$) to yield

$$\frac{d\theta_{A^*-B^*}}{dt} = 0 = k_{A,ads}P_A\theta_{B^*} - k_{A,des}\theta_{A^*-B^*} + 3k_{B_2,ads}P_{B_2}\theta_{A^*} - 3k_{B_2,des}\theta_{B^*}\theta_{A^*-B^*} - k_{sr}\theta_{A^*-B^*} \quad \textbf{[37]}$$

We now rearrange and solve for $\theta_{A^*-B^*}$

$$\theta_{A^*-B^*} = \frac{k_{A,ads}P_A\theta_{B^*} + 3k_{B_2,ads}P_{B_2}\theta_{A^*}}{k_{A,des} + 3k_{B_2,des}\theta_{B^*} + k_{sr}} \quad \textbf{[38]}$$

which, dividing numerator and denominator by $k_{B_2,des}$, is

$$\theta_{A^*-B^*} = \frac{\frac{k_{A,ads}P_A\theta_{B^*}}{k_{B_2,des}} + \frac{3k_{B_2,ads}P_{B_2}}{k_{B_2,des}}\theta_{A^*}}{\frac{k_{A,des}}{k_{B_2,des}} + 3\theta_{B^*} + \frac{k_{sr}}{k_{B_2,des}}} \quad \textbf{[39]}$$

Again evoking Conditions (I) and (II) and collecting terms gives

$$\theta_{A^*-B^*} = \frac{\theta_{A^*}\theta_{B^*}\left(\frac{k_{A,des}}{k_{B_2,des}} + 3\theta_{B^*}\right)}{\left(\frac{k_{A,des}}{k_{B_2,des}} + 3\theta_{B^*}\right) + \frac{k_{sr}}{k_{B_2,des}}} \quad \textbf{[40]}$$

Eq. **38** is the most general closed-form solution for $\theta_{A^*-B^*}$ under Conditions (I) and (II) and is only further simplified by recognizing that $3\theta_{B^*} << k_{A,des}/k_{B_2,des} \sim 1$ per Table 3, permitting accurate redaction to

$$\theta_{A^*-B^*} = \frac{\theta_{A^*}\theta_{B^*}}{1 + \frac{k_{sr}}{k_{A,des}}} \quad \textbf{[41]}$$

From re-arrangement of Eq. **41**, we see

$$\mu_{A^*-B^*} \equiv \frac{\theta_{A^*-B^*}}{\theta_{A^*}\theta_{B^*}} = \frac{1}{1 + \frac{k_{sr}}{k_{A,des}}} \quad \textbf{[42]}$$

indicating $k_{sr}/k_{A,des}$ is the salient parameter in determining the profundity of ensemble site-size effects under Conditions (I) and (II).

If $k_{sr} >> k_{A,des}$, A^*–B^* reaction out-competes sorption-mediated conveyance of A^* and effects a 'transport limited' surface. If $k_{sr} << k_{A,des}$, A^* desorption and re-adsorption provides a rapid means of A^*–B^* generation, precipitating a 'surface-reaction limited' catalytic rate and random adsorbate distribution. Table 3 confirms $k_{sr} >> k_{A,des}$ in this case study, from which we derive the remarkable result

$$R_{AB_{(g)},1st} = 4k_{A,des}K_A P_A \sqrt{K_{B_2} P_{B_2}} \quad \textbf{[43]}$$

in which the rate constant of surface reaction does not appear and is replaced by $k_{A,des}$. Consequently, we surmise (i) $A_{(g)}$ adsorption is *both equilibrated and rate-determining* and (ii) the Langmuir-Hinshelwood formalism erroneously calculates elementary step activation parameters in accordance with the erroneous identification of surface reaction as the rate-determining step.

We explicate miscalculation of activation enthalpies and entropies in the following by fit of 'rate data' calculated by the full first-order microkinetic model with transition-state theory (TST) forms of closed-form expressions for rate

$$R_{AB_{(g)}} = \frac{4k_BT}{h} P_A \sqrt{P_{B_2}} e^{\frac{\Delta S_{app}^{0,\ddagger}}{k_B N_{Av}} - \frac{\Delta H_{app}^{0,\ddagger}}{k_B N_{Av}}\left(\frac{1}{T}\right)} \quad \textbf{[44]}$$

where k_B and h are the Boltzmann and Planck constants respectively. Apparent activation parameters $\Delta S_{app}^{0,\ddagger}$ and $\Delta H_{app}^{0,\ddagger}$ are respectively

$$\Delta S_{app}^{0,\ddagger} = \Delta S_{rds}^{0,\ddagger} + \Delta S_{A,ads}^{0} + \frac{1}{2}\Delta S_{B_2,ads}^{0} \quad \textbf{[45]}$$

and

$$\Delta H_{app}^{0,\ddagger} = \Delta H_{rds}^{0,\ddagger} + \Delta H_{A,ads}^{0} + \frac{1}{2}\Delta H_{B_2,ads}^{0} \quad \textbf{[46]}$$

and describe the thermodynamic driving forces dictating equilibrium between the most populous stable initial states (i.e. $A_{(g)}$ and $B_{2(g)}$) and the rate-controlling transition state. We note that the statistical factor '4' in Eq. **44**, correspondent to coordination of a square lattice, is easily forgotten in TST-formulation of reaction rates and is required to accurately quantify entropic changes from the initial to transition state.

From transition-state theory, the apparent equilibrium between the transition state and reactants can be quantified as

$$ln(K^{\ddagger}) = ln\left(\frac{a_{app}^{\ddagger}}{P_A\sqrt{P_{B_2}}}\right) \equiv \frac{\Delta S_{app}^{0,\ddagger}}{k_B N_{Av}} - \frac{\Delta H_{app}^{0,\ddagger}}{k_B N_{Av}}\left(\frac{1}{T}\right) = ln\left(\frac{R_{AB_{(g)}}}{\frac{4k_BT}{h}P_A\sqrt{P_{B_2}}}\right) \quad \textbf{[47]}$$

where $a^{\ddagger}$ is the thermodynamic activity of the apparent (i.e. rate-determining) transition state, activities of ideal gas-phase species $A_{(g)}$ and $B_{2(g)}$ are equal to partial pressures normalized by 1 bar, and N_{Av} is the Avogadro constant. Fit of zeroth-order (Eq. **33**) and first-order rate (Eq. **43**) expressions in the form of Eq. **47** determines $\Delta S_{rds}^{0,\ddagger}$ and $\Delta H_{rds}^{0,\ddagger}$ – provided standard state sorption

enthalpies and entropies are measured *ex situ* (e.g. by microcalorimetry [43–45]) or are reliably calculated (e.g. by density functional theory [45]).

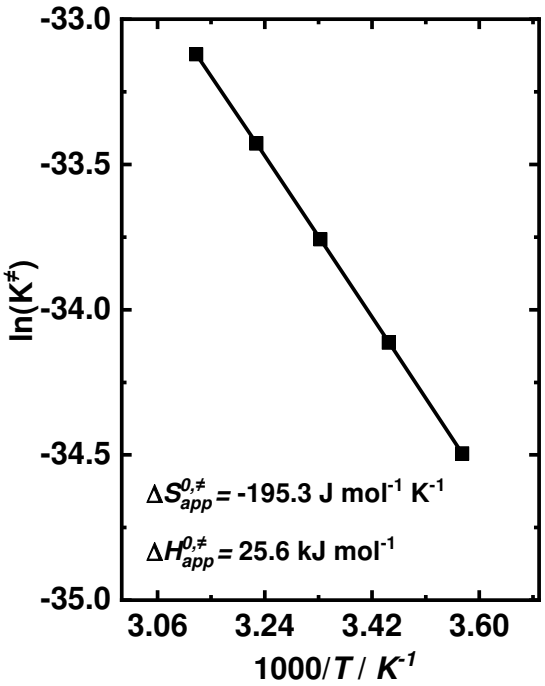

Fig. 5: Apparent transition-state equilibrium constant, $K^{\ddagger}$, calculated by the full first-order microkinetic model method (■) as a function of T^{-1} for $P_A = 10^{-6}$ bar and $P_{B_2} = ½ \times 10^{-3}$ bar. 'Rate data' (■) are fit to Eq. **47** (—) to calculate apparent activation parameters $\Delta S_{app}^{0,\ddagger}$ and $\Delta H_{app}^{0,\ddagger}$.

Figure 5 shows $ln(K^{\ddagger})$ calculated by the full first-order microkinetic model and fit by Eq. **47** for T = 280 K – 320 K. Closed-form rate expressions in the zeroth order (Eq. **33**) and first order (Eq. **43**) are identical, save for respective linearity with respect to k_{sr} and $k_{A,des}$, and, therefore, both formalisms calculate, per Eqs. **45**-**46**, $\Delta S_{rds}^{0,\ddagger}$ = 26.2 J mol^{-1} K^{-1} and $\Delta H_{rds}^{0,\ddagger}$ = 64.2 kJ mol^{-1} which deviate negligibly from $A_{(g)}$ desorption activation parameters because $A_{(g)}$ sorption is nearly-entirely rate-determining (i.e. $X_{RC,A,ads} \sim 0.95$). The Langmuir-Hinshelwood formalism, however, misidentifies *rds* = *sr*, and consequently mistakenly attributes the entropic gain of 26.2 J mol^{-1} K^{-1} to the associative formation of the $(A^*–B^*)^{\ddagger}$ transition state which, in actuality, is

formed with an entropic loss of –8.3 J mol^{-1} K^{-1}. The identical quantitative fits but disparate physical interpretation of zeroth- and first-order rate expressions highlight the unreliability of goodness-of-fit to assess the veracity of a kinetic model. Accurate predictions of $A_{(g)}$ and $B_{2(g)}$ reaction orders and quantitative fit to temperature-dependent rate data do not guarantee appropriateness of Langmuir-Hinshelwood or any other kinetic formalism. Instead, the veracity and reliability of a kinetic description is predicated on (i) the fidelity with which the mathematical formulation of the theory describes its foundational physical precepts and (ii) the extent to which the physical precepts of a theory agree with the considered natural phenomenon. In the case of the Langmuir-Hinshelwood formalism, the approximation $\mu_{ij} = 1$ fundamentally conflicts with (i + ii) the established ability of Langmuirian adsorbates to diffuse with non-infinite rate and proscribes reliable application of the formalism to describe any catalytic system without known infinitely-fast diffusion of all surface species.

The immobility of adsorbates in the $A + ½B_2 \rightarrow AB$ reaction is incognizable to the Langmuir-Hinshelwood formalism and is responsible for the ascription of $\Delta S_{rds}^{0,\ddagger} = 26.2$ J mol^{-1} K^{-1} to the surface reaction step which instead forms the $(A^*–B^*)^\ddagger$ transition state with an entropic loss. Misattribution of intrinsic entropic activation barriers to surface reaction therefore fundamentally misrepresents entropic drivers for the formation of the ostensibly rate-controlling $(A^*–B^*)^\ddagger$ transition state. Similarly, enthalpic barriers to $(A^*–B^*)^\ddagger$ formation are overestimated by 18.5 kJ mol^{-1} – a profound miscalculation given the apparent simplicity of the reaction network and quantitative zeroth-order fit. In actuality, as the first-order formalism correctly describes, the calculated rate-controlling entropic and enthalpic barriers reflect activation energetics of A^* desorption responsible for liberating immobile, isolated A^* only allied to B^* by $A_{(g)}$ re-adsorption with rate $r_{A,ads,[A^*–B^*]} = k_{A,ads}P_A\theta_{B^*} = k_{A,des}P_AK_A(K_{B_2}P_{B_2})^{½} = ¼\ R$. In this sense, the rate-

determining step is, most specifically, the irreversible, two-site adsorption event $A_{(g)} + B^*–* \rightarrow A^*–B^*$ which exemplifies the critical importance of first-order description of ostensibly single-site elementary steps (e.g. $A_{(g)}$ adsorption) which may control rates via an ensemble-specific two-site path.

The limitations of the Langmuir-Hinshelwood model responsible for unfaithful description of the $A + ½B_2 \rightarrow AB$ reaction are entirely resolved by arbitrarily-fast surface diffusion which rids $A_{(g)}$ sorption of the kinetic burden to generate $A^*–B^*$ pairs. However, as we describe in the following, infinitely-fast surface diffusion is insufficient to guarantee accuracy of the Hinshelwood approximation if adsorbed species occupy more than one site.

3.3 Case Study III: Kinetic consequences of two-site associative B_2 adsorption in $A + B_2 \rightarrow AB_2$

Catalytic chemistries which (de-)hydrogenate, fragment, and/or grow hydrocarbon chains commonly involve multi-site-occupying intermediates which arbitrate rates of kinetically-relevant and selectivity-determining steps [3,4,7,18,47–49]. Multi-site occupation of reactive intermediates confers an inherent clustering of constituent fragments (e.g. CH_2^* in $^*CH_2CH_2^*$) indescribable by zeroth- or first-order truncation procedures. Challenges in analytically describing catalysis of multi-site occupants arise from difficulty in distinguishing between (i) unbound, neighboring fragments that are facilely unpaired (e.g. $CH_2^*CH_2^*$) and (ii) bonded fragments that constitute a single adspecies which cannot be disassembled (e.g. $^*CH_2CH_2^*$). Inseparability of bound methylene moieties in adsorbed ethylene is formulated analytically by prohibition of ensembles and ensemble-specific elementary steps which wrongly isolate CH_2^*. Specification of precluded ensembles requires a second-order kinetic description to wholly retain

and bar configurations such as *–CH_2^*–* on linear lattices and analogous five-site ensembles which strand CH_2^* on square lattices.

Scheme 6: Ensembles forbidden in catalytic ethylene hydrogenation[†]

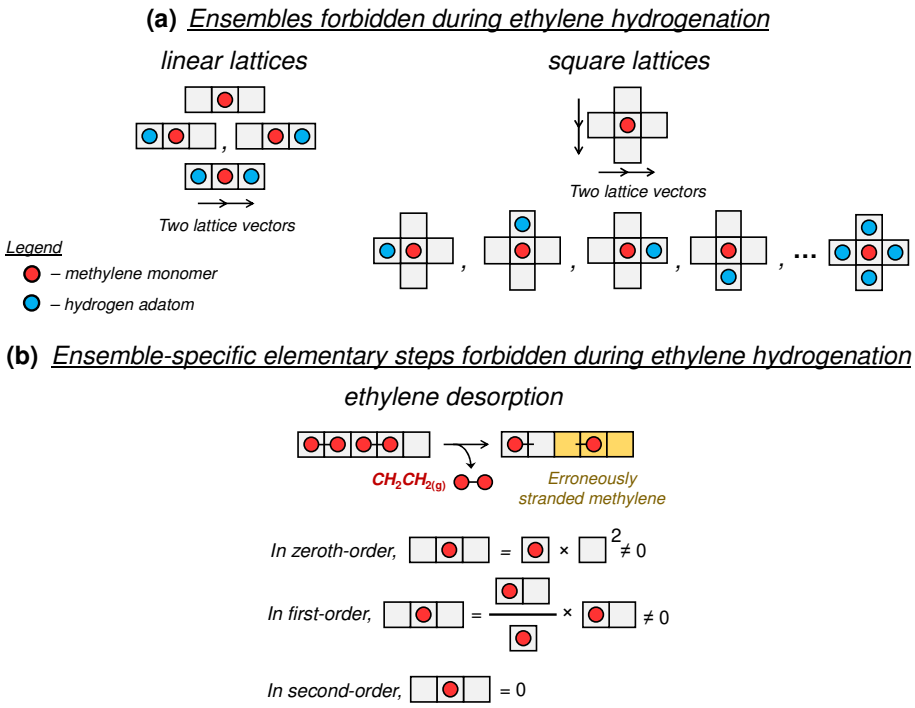

[†](a) Ensembles on linear and square lattices which isolate monomeric methylene fragments (●) and are erroneously permitted in zeroth- and first-order truncations. Two lattice vectors are needed to wholly retain each ensemble and, therefore, a ≥second-order truncation procedure is required. (b) Elementary step events which wrongly strand monomeric methylene fragments. Zeroth- and first-order ensembles are unable to specify $\theta_{*\text{–}CH2*\text{–}*} = d\theta_{*\text{–}CH2*\text{–}*}/dt = 0$ and, therefore, permit the illustrated ethylene desorption event.

Scheme 6 illustrates such forbidden ensembles in the context of catalytic ethylene hydrogenation and explicates the necessity of the second-order truncation procedure. Zeroth- and first-order methods erroneously permit elementary steps such as ethylene desorption to segregate bonded $^{*}CH_2CH_2{}^{*}$ pairs, as shown in Scheme 6, and, consequently, predict non-physical isolation of methylene fragments in hydrogenation reactions. Explicit retention of three-site configurations in the second order is a pre-requisite for disallowing methylene isolation (e.g. via ethylene desorption) and is critical to quantitatively distinguishing between coverages of compositionally-identical but chemically-distinct $CH_2{}^{*}CH_2{}^{*}$ and $^{*}CH_2CH_2{}^{*}$ ensembles.

Table 5: Horiuti-Polanyi-type reaction of a two-site-occupying adsorbate

#	Step	Rate constants
1	$A_{2(g)} + * - * \rightarrow {}^{*}AA^{*}$	$k_{A_2,ads}$= 1 (bar · s)$^{-1}$
–1	${}^{*}AA^{*} \rightarrow A_{2(g)} + * - *$	$k_{A_2,des}$ = 1 s^{-1}
2	$B_{2(g)} + * - * \rightarrow B^{*} - B^{*}$	$k_{B_2,ads}$= 1 (bar · s)$^{-1}$
–2	$B^{*} - B^{*} \rightarrow B_{2(g)} + * - *$	$k_{B_2,des}$ = 1 s^{-1}
3	${}^{*}AA^{*} - B^{*} \rightarrow A_2B_{(g)} + * - * - *$	k_{sr} = 1 s^{-1}
n/a	${}^{*}AA^{*} - * \leftrightarrow * - {}^{*}AA^{*}$	$k_{A,diff} \geq 10^5$ s^{-1}
n/a	$B^{*} - * \leftrightarrow * - B^{*}$	$k_{B,diff} \geq 10^5$ s^{-1}

We explicate second-order distinction between bonded and unbound surface fragments in the context of a simple, generic Horiuti Polanyi mechanism analogous to catalytic ethylene hydrogenation [50–53]. The hydrogenation-type mechanism $A_2 + B_2 \rightarrow A_2B$ occurs on a linear lattice via the sequence of elementary steps in Table 5 wherein (i) the adsorbed analog of $A_{2(g)}$, ${}^{*}AA^{*}$, occupies two sites analogously to ${}^{*}CH_2CH_2{}^{*}$, (ii) $B_{2(g)}$ adsorbs dissociatively analogously to molecular hydrogen, and (iii) diffusion of all adsorbates is arbitrarily-fast compared to catalysis. The intrinsic non-randomness conferred by inseparable ${}^{*}AA^{*}$ pairs is not facilely overcome by surface diffusion and requires $k_{diff}/k_{i\neq diff} \geq 10^5$ to be regarded infinitely-fast – a condition we quantitatively confirm by calculation of ensemble-specific diffusion reversibilities, as detailed in Section S3. Bonded ${}^{*}AA^{*}$ pairs and unbound $A^{*}A^{*}$ ensembles are of identical occupancy and, therefore, are not naturally distinguished by the second order truncation procedure; instead, the distinction between these ensembles must be enforced by explicit prohibition of three-site ensembles which isolate A^{*}

$$\theta_{*-A^{*}-*} = \theta_{B^{*}-A^{*}-*} = \theta_{B^{*}-A^{*}-B^{*}} = 0 \qquad \textbf{[48]}$$

Non-random ensemble constraints described by Eq. **48** effect configurational non-idealities in the distribution of all other ensembles, as captured by second-order site balances akin to first-order balances in Eq. **10**

$$\theta_{ij} = \sum_{\substack{k=site \\ occupants}} \theta_{ijk} = \sum_{\substack{m=site \\ occupants}} \theta_{mij} \qquad \textbf{[49]}$$

where *k* and *m* are indices over all single-site occupants. Diametric placement of *k* and *m* on either side of the *ij* pair gives distinct ensemble balances without analogy in zeroth- and first-order methods. For example, Eq. **49** gives two distinct balances on A^*–B^* pairs

$$\theta_{A^*-B^*} = \sum_{\substack{m=site \\ occupants}} \theta_{m-A^*-B^*} = \theta_{A^*-A^*-B^*} + \theta_{B^*-A^*-B^*} + \theta_{*-A^*-B^*} = \theta_{A^*-A^*-B^*} \qquad \textbf{[50]}$$

which reduces to a single term per Eq. **48**, and

$$\theta_{A^*-B^*} = \sum_{\substack{k=site \\ occupants}} \theta_{A^*-B^*-k} = \theta_{A^*-B^*-A^*} + \theta_{A^*-B^*-B^*} + \theta_{A^*-B^*-*} \qquad \textbf{[51]}$$

which retains three coverage terms – none of which appear in Eq. **50**. In this way, the second-order formalism describes two-site ensembles with spatial detail which (i) is lost in ≤first-order truncation procedures and (ii) provides information critical to describing non-random distribution and chemical dynamics of kinetically-relevant ensembles such as the reactive A^*–A^*–B^* configuration derived to be equal in population to the two-site A^*–B^* pair (Eq. **50**). Analogous second-order balance on A^*–* pairs gives $\theta_{A^*-*} = \theta_{A^*-A^*-*}$ from which we derive a simplified balance on $\theta_{A^*-A^*}$, the total coverage of as-yet undistinguished bonded and unbound A^* pairs

$$\theta_{A^*-A^*} = \sum_{\substack{m=site \\ occupants}} \theta_{m-A^*-A^*} = \theta_{A^*-B^*} + \theta_{A^*-*} + \theta_{A^*-A^*-A^*} \qquad \textbf{[52]}$$

Eq. **52** provides a constraint on populations of all two-site A^*-containing ensembles, motivating combination with the first-order balance

$$\theta_{A^*} = \sum_{\substack{k=site \\ occupants}} \theta_{A^*-k} = \theta_{A^*-B^*} + \theta_{A^*-*} + \theta_{A^*-A^*} \quad \textbf{[53]}$$

Eqs. **52** and **53** communicate distinct, complementary spatial information, the concert of which reveals that the coverage of all A^*–A^* ensembles is the sum of two terms

$$\theta_{A^*-A^*} = \frac{\theta_{A^*}}{2} + \frac{\theta_{A^*-A^*-A^*}}{2} \quad \textbf{[54]}$$

each accounting for a chemically-distinct A^*–A^* pair. Eq. **54** is only derivable because of the spatial detail captured by the second-order balance (Eq. **52**) and makes clear that (i) $\theta_{*AA*} = ½\theta_{A*}$ consistent with the stoichiometry of $^*AA^*$ species and (ii) $\theta_{A*A*} = ½\theta_{A*-A*-A*}$ because neighboring, unbound A^* must be members of distinct $^*AA^*$ adsorbates. From Eq. **54**, the absolute lower bound on the coverage of all A^*–A^* ensembles is evidently $(\theta_{A*-A*})_{min} = \theta_{*AA*} = ½\theta_{A*}$ corresponding to surfaces wherein no adsorbed analogs of $A_{2(g)}$ neighbor one another. The two-site occupancy of $^*AA^*$ species therefore prescribes an absolute lower bound on the mean-field metric of A^*–A^* pairs

$$(\mu_{A^*-A^*})_{min} \equiv \frac{(\theta_{A^*-A^*})_{min}}{\theta_{A^*}^2} = \frac{1}{2 \cdot \theta_{A^*}} \quad \textbf{[55]}$$

which demands $\mu_{A*-A*} > 1$ for $\theta_{A*} < ½$ – excluding accuracy of the Hinshelwood approximation (i.e. $\mu_{ij} = 1$) even if surface diffusion of all adspecies is arbitrarily-fast. We therefore surmise that there is no condition which permits reliable use of the zeroth-order formalism to describe catalytic sequences involving ≥two-site-occupying surface intermediate(s) – as we demonstrate by comparison of zeroth-order (Table 6) and second-order (Table 7) microkinetic models in what follows.

We report elementary step rates for select ensembles in Tables 7(A) and 7(B) which provide a representative sample of the complexity and variety of rate terms retained in the second order formalism. A complete description of the second-order treatment is provided in Section S3.

Table 6: Langmuir-Hinshelwood rate equations for Horiuti-Polanyi reaction $A_2 + B_2 \rightarrow A_2B$

Langmuir-Hinshelwood							
Step, i	$A_{2(g)}$ *ads.*	$A_{2(g)}$ *des.*	$B_{2(g)}$ *ads.*	$B_{2(g)}$ *des.*	*reaction*	A^* *diffusion*	B^*-B^* *diffusion*
Rate, r_i	$k_{A_2,ads}P_{A_2}\theta_*^2$	$k_{A_2,des}\theta_{A^*}^2$	$k_{B_2,ads}P_{B_2}\theta_*^2$	$k_{B_2,des}\theta_{B^*}^2$	$k_{sr}\theta_{A^*}^2\theta_{B^*}$	$k_{A,diff}\theta_{A^*}^2\theta_*$	$k_{B,diff}\theta_{B^*}\theta_*$
Ensemble-Specific Stoichiometric Coefficients							
$\boldsymbol{\nu_{i,[A^*]}}$	2	– 2	0	0	– 4	0	0
$\boldsymbol{\nu_{i,[A^*-B^*]}}$	No explicit rate equations. $\theta_{ij} = \theta_i\theta_j$						
$\boldsymbol{\nu_{i,[*-*-*]}}$	No explicit rate equations. $\theta_{ijk} = \theta_i\theta_j\theta_k$						

Rate equations for each ensemble and each elementary step are constructed by product of the fundamental rate of the step (e.g. $k_{B_2,ads}P_{B_2}\theta_*^2$ for $B_{2(g)}$ adsorption) and the corresponding ensemble-specific stoichiometric coefficient (e.g. 2 for B^* for $B_{2(g)}$ adsorption).

Table 7(A): Second-order rate equations for Horiuti-Polanyi reaction $A_2 + B_2 \rightarrow A_2B$

Second-order				
Step, i	$A_{2(g)}$ *ads.*	$A_{2(g)}$ *des.*	$B_{2(g)}$ *ads.*	$B_{2(g)}$ *des.*
Rate, r_i	$k_{A_2,ads}P_{A_2}\theta_{*-*}$	$k_{B_2,des}\theta_{A^*-A^*}$	$k_{B_2,ads}P_{B_2}\theta_{*-*}$	$k_{B_2,des}\theta_{B^*-B^*}$
Ensemble-Specific Stoichiometric Coefficients				
$\boldsymbol{\nu_{i,[A^*]}}$	2	– 2	0	0
$\boldsymbol{\nu_{i,[A^*-B^*]}}$	$\frac{\theta_{B^*-*-*}}{\theta_{*-*}}$	$-\frac{\theta_{B^*-A^*-A^*}}{\theta_{A^*-A^*}}$	$\frac{\theta_{A^*-*-*}}{\theta_{*-*}}$	$-\frac{\theta_{A^*-B^*-B^*}}{\theta_{B^*-B^*}}$
$\boldsymbol{\nu_{i,[*-*-*]}}$	$-2\frac{\theta_{*-*-*}}{\theta_{*-*}} - 2\frac{\theta_{*-*-*}^2}{\theta_{*-*}^2}$	$2\frac{\theta_{A^*-A^*-*}}{\theta_{A^*-A^*}} + 2\frac{\theta_{A^*-A^*-*}\theta_{A^*-*-*}}{\theta_{A^*-A^*}\theta_{A^*-*}}$	$-2\frac{\theta_{*-*-*}}{\theta_{*-*}} - 2\frac{\theta_{*-*-*}^2}{\theta_{*-*}^2}$	$2\frac{\theta_{B^*-B^*-*}}{\theta_{B^*-B^*}} + 2\frac{\theta_{B^*-B^*-*}\theta_{B^*-*-*}}{\theta_{B^*-B^*}\theta_{B^*-*}}$

Rate equations for each ensemble and each elementary step are constructed by product of the fundamental rate of the step (e.g. $k_{B_2,ads}P_{B_2}\theta_{*-*}$ for $B_{2(g)}$ adsorption) and the corresponding ensemble-specific stoichiometric coefficient (e.g. $\theta_{A^*-*-*}/\theta_{*-*}$ for A^*–B^* for $B_{2(g)}$ adsorption).

Table 7(B): Second-order rate equations for Horiuti-Polanyi reaction $A_2 + B_2 \rightarrow A_2B$

Second-order			
Step, i	*reaction*	A^* *diffusion*	B^*-B^* *diffusion*
Rate, r_i	$k_{sr}\theta_{A^*-A^*-B^*}$	$k_{A,diff}\theta_{A^*-A^*-*}$	$k_{B,diff}\theta_{B^*-*}$
Ensemble-Specific Stoichiometric Coefficients			
$\boldsymbol{\nu_{i,[A^*]}}$	-4	0	0
$\boldsymbol{\nu_{i,[A^*-B^*]}}$	$-1-\frac{\theta_{A^*-B^*-A^*}}{\theta_{A^*-B^*}}-\frac{\theta_{B^*-A^*-A^*}}{\theta_{A^*-A^*}}$	$\frac{\theta_{A^*-*-B^*}}{\theta_{A^*-*}}-\frac{\theta_{B^*-A^*-A^*}}{\theta_{A^*-A^*}}$	$\frac{\theta_{A^*-*-B^*}-\theta_{A^*-B^*-*}}{\theta_{B^*-*}}$
$\boldsymbol{\nu_{i,[*-*-*]}}$	$2\left(1+\frac{\theta_{A^*-B^*-*}}{\theta_{A^*-B^*}}+\frac{\theta_{A^*-A^*-*}}{\theta_{A^*-A^*}}+\frac{\theta_{A^*-B^*-*}\theta_{B^*-*-*}}{\theta_{A^*-B^*}\theta_{B^*-*}}+\frac{\theta_{A^*-A^*-*}\theta_{A^*-*-*}}{\theta_{A^*-A^*}\theta_{A^*-*}}\right)$	$2\frac{\theta_{A^*-A^*-*}\theta_{A^*-*-*}}{\theta_{A^*-A^*}\theta_{A^*-*}}-2\frac{\theta_{A^*-*-*}\theta_{*-*-*}}{\theta_{A^*-*}\theta_{*-*}}$	$2\frac{\theta_{B^*-*-*}\theta_{*-B^*-*}}{\theta_{B^*-*}^2}-2\frac{\theta_{*-*-*}\theta_{B^*-*-*}}{\theta_{*-*}\theta_{B^*-*}}$

Rate equations for each ensemble and each elementary step are constructed by product of the fundamental rate of the step (e.g. $k_{B,diff}\theta_{B^*-*}$ for B^* diffusion) and the corresponding ensemble-specific stoichiometric coefficient (e.g. $[\theta_{A^*-*-B^*} - \theta_{A^*-B^*-*}]/\theta_{B^*-*}$ for A^*–B^* for B^* diffusion).

Figure 6 compares mean-field metrics, coverages, reaction orders, and degrees of rate control calculated by the zeroth- and second-order microkinetic models as a function of P_{A_2} using rate constants listed in Table 5. Surface diffusion of $^*AA^*$ and B^* is confirmed to be infinitely-fast by calculation of ensemble-specific diffusion reversibilities – all of which are unity – and by invariance of all kinetic parameters with increase to $k_{A,diff}$ or $k_{B,diff}$ (Section S3). Fig. 6(A) demonstrates infinitely-fast adsorbate diffusion is incapable of guaranteeing $\mu_{A^*-A^*} = 1$ for $A_{2(g)}$ pressures sufficiently low to effect $\theta_{A^*} < ½$ (Fig. 6(B)). The second-order formalism correctly captures the precipitous increase of $\mu_{A^*-A^*}$ as A^* coverage is decremented and intrinsic clustering of $^*AA^*$ compels supra-random A^* aggregation. Second-order calculations of $\mu_{A^*-A^*}$ slightly exceed $(\mu_{A^*-A^*})_{min} = ½\theta_{A^*}^{-1}$ because of the small contribution of unbound A^*A^* pairs.

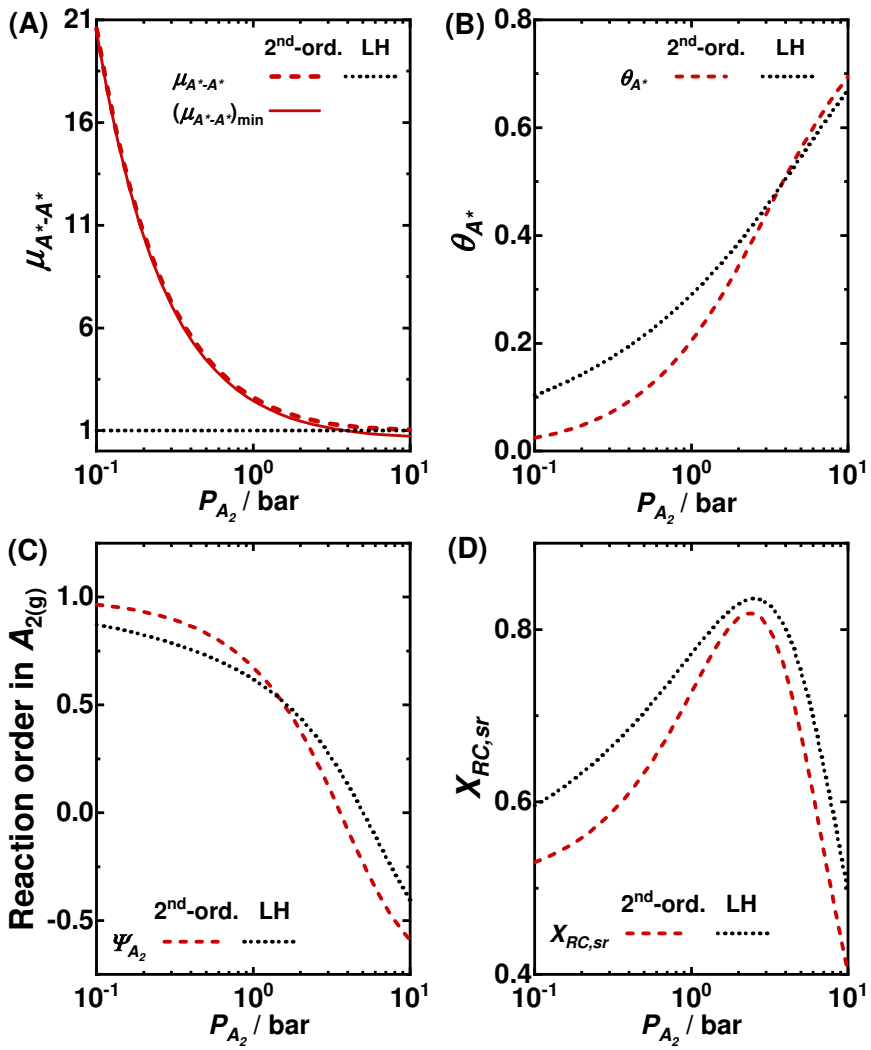

Fig. 6: (A) Mean-field metric of A^* pairs, $\mu_{A^*\text{–}A^*}$, calculated by Langmuir-Hinshelwood (···) and second-order (---) formalisms and compared to the absolute lower bound $(\mu_{A^*\text{–}A^*})_{min} = (2\theta_{A^*})^{-1}$ (—) per Eq. **53**. (B) Fractional coverage of A^*-occupied sites, (C) reaction order in $A_{2(g)}$, and (D) degree of rate control of surface reaction calculated by Langmuir-Hinshelwood (···) and second-order (---) formalisms. Calculations are of the reaction network in Table 5 with $P_{B_2} = 1$ bar.

Total coverages of A^* fragments are profoundly overestimated by the Langmuir-Hinshelwood model for $P_{A_2} < 1$ bar. The Hinshelwood approximation $\mu_{A^*\text{–}A^*} = 1$ becomes increasingly poor as $\theta_{A^*} \rightarrow 0$ and, as a result, the rate of A^* consumption $r = k_{sr}\theta_{A^*}{}^2\theta_{B^*}$ is underestimated – effecting an erroneous accumulation of A^* species which, in actuality, react rapidly because of the ensured proximity of a bonded A^* species (i.e. ${}^*AA^*$ adspecies prescribe $\theta_{A^*\text{–}A^*\text{–}B^*}/\theta_{A^*\text{–}B^*} = 1 \neq \theta_{A^*}$).

Invalidity of the $\theta_{A^*-A^*-B^*}/\theta_{A^*-B^*} = \theta_{A^*}$ approximation is unresolved by surface diffusion at all coverages and, consequently, reaction orders in $A_{2(g)}$ and degrees of rate control of surface reaction are generally miscalculated by the Langmuir-Hinshelwood method (Figs. 6(C) and 6(D)). In this way, the inability of ≤first-order formalisms to inventory $^*A\text{-}A^*$ bonds begets uncertainty in all kinetic descriptors – despite the ostensible capacity of surface diffusion to randomize adsorbate distribution. Intrinsic non-randomness conferred by $^*AA^*$ two-site occupancy cannot be overcome by any set of rate parameters and is only reliably neglected on $^*AA^*$-saturated surfaces which warrant $\theta_{A^*-A^*-B^*}/\theta_{A^*-B^*} = \theta_{A^*} = 1$. We therefore caution against use of the Langmuir-Hinshelwood formalism to describe any catalytic sequence mediated by multi-site occupants and advocate efforts to develop and computationally implement higher-order formalisms for general use in the description of catalytic surface reactions.

4. Discussion

…

In an effort to preempt misconception of the higher-order kinetic formalism described in this work, we discuss and reiterate below a selection of key concepts related to the definition of site ensembles and the scope and application of the presented kinetic framework.

4.1 Definition of catalytic site ensembles

We define a site ensemble to be a collection of sites which (i) are contiguous and (ii) each have a specified occupancy. A site ensemble is therefore identified by its connectivity (i.e. size and shape) and composition (i.e. occupation of each site). For example, distinct site ensembles $A^*–A^*$ and *–* are identical in connectivity and are distinguished by composition. Conversely,

distinct site ensembles A^*–A^*–A^* and $\begin{matrix} A^* - A^* \\ \quad\quad\ | \\ \quad\quad A^* \end{matrix}$ are identical in composition and are distinguished by connectivity.

We stress that ensembles of disparate size and identical composition (i.e. * and *–*) do not refer to distinct sites of different nuclearity or spatial extent. That is to say, * and *–* do not refer, as an example, to atop and hollow sites, respectively. Ensembles of multiple *types* of sites (e.g. $*_{atop}$–$*_{hollow}$) are not addressed in this work; however, we hope to illustrate in future studies that the combined chemical and spatial specificity proffered by the higher-order kinetic formalism we present herein is uniquely suited to describe the dynamics of ensembles of multiple types of sites (e.g. on metal alloy catalysts [54,55]).

4.2 Thermodynamic non-idealities*: *lateral adsorbate interactions

The primary development of this work is provision of a reliable method by which to enumerate ≥two-site ensemble populations on any catalytic surface. Although we present the mathematical framework in the context of Langmuirian surfaces and species, Conditions (I)-(III) are not a pre-requisite of the described method. Hierarchical rate equations constructed by enumeration and truncation of conditional probabilities may be derived even if (i) the absorbent/catalytic surface contains an arbitrary distribution of an arbitrary number of sites, (ii) each site can accommodate more than one occupant, or (iii) adsorbed species energetically interact.

The incorporation of each of these non-idealities into higher-order descriptions requires an increment in the amount of retained information and, therefore, an increment in the number of independent variables. To explicate the capacity of the higher-order method to account for such

non-idealities – and the attendant increase in complexity – we detail inclusion of lateral adsorbate interactions into a first-order description of $A_{(g)}$ desorption on a 2D square lattice.

We introduce thermodynamic non-idealities by considering adjacent A^* species to interact with energy $\varepsilon_{A^*-A^*}$. For simplicity, we regard vacant sites and transition states as non-interacting – a condition which is relaxed in a more general treatment of adsorbate interactions in our recent work [12]. The kinetic consequences of A^*–A^* energetic interactions are determined by (i) the polarity and strength of interaction, quantified by $\varepsilon_{A^*-A^*}$, and (ii) the frequency of interaction, quantified by $\theta_{A^*-A^*}$. An analytical treatment of nearest-neighbor adsorbate interactions therefore requires reliable enumeration of A^*–A^* pairs – as is achieved by the first-order method.

Previous attempts to analytically describe thermodynamic non-idealities rely on approximations which, similarly to the Hinshelwood approximation, enable site-pair populations to be expressed in terms of single-site coverages. The quasi-chemical approximation (QCA) [22,56,57], for example, assumes the surface is energetically-equilibrated and correspondingly applies the thermodynamic constraint

$$\frac{\theta_{A^*-*}^2}{\theta_{A^*-A^*}\theta_{*-*}} = e^{\epsilon_{A^*-A^*}/k_BT} \qquad \textbf{[58]}$$

which, coupled to site and component balances, is sufficient to reduce the number of independent ensembles to 5 – 4 = 1, meaning a microkinetic model only requires rate equations for A^* or *. The equilibrium condition in Eq. **58**, however, is only applicable if surface diffusion is infinitely-fast compared to catalysis and ensures the adsorbate distribution energetically equilibrates. In this sense, QCA is a generalization of the Hinshelwood approximation to thermodynamically non-ideal surfaces. A general description of lateral adsorbate interactions requires $\theta_{A^*-A^*}$ be retained as an independent variable and be described by ensemble-specific thermodynamically non-ideal rate equations.

Consider, for example, desorption of A^* from a square lattice. The desorbing A^* species has m = 0, 1, 2, 3, or 4 nearest-neighboring A^* species. The number of A^*–A^* pairs eliminated by desorption affects the energy of the desorbing initial state relative to the transition state and, therefore, alters the effective activation energy of desorption. The rate of desorption with m neighboring A^* species is therefore

$$r_{des,\{m\}} = \omega_{des,\{m\}} \times k_{des} e^{\frac{m\epsilon_{A^*-A^*}}{k_B T}} \theta_{des,m} \qquad \textbf{[59]}$$

where k_{des} is the thermodynamically-ideal desorption rate constant, $\theta_{des,m}$ is the coverage of five-site desorptive configurations with exactly m neighboring A^* species, and $\omega_{des,\{m\}}$ is the multiplicity of five-site desorptive configurations with exactly m neighboring A^* species. For example, for m = 3,

$$r_{des,\{3\}} = 4k_{des} e^{\frac{3\epsilon_{A^*-A^*}}{k_B T}} \theta_{\substack{A^* \\ | \\ A^*-A^*-* \\ | \\ A^*}} \qquad \textbf{[60]}$$

where $\omega_{des,\{3\}}$ = 4 because the neighboring * site may be at any of the four positions neighboring the central, desorbing A^* species. The rate of desorption is a sum of terms analogous to Eq. **60** for m = 0 to m = 4 which, after execution of the first-order truncation procedure, gives

$$r_{des} = k_{des}\theta_{A^*}\left[\frac{\theta_{A^*-A^*}e^{\frac{\epsilon_{A^*-A^*}}{k_B T}} + \theta_{A^*-*}}{\theta_{A^*}}\right]^4 \qquad \textbf{[61]}$$

The bracketed term compendiously captures the propensity of lateral adsorbate interactions to affect the activation energy of desorption and is referred to in the following as Γ_{des}. The interaction term Γ_{des} is a function of $\theta_{A^*-A^*}$ and θ_{A^*-*} and therefore couples to rate equations for two-site ensembles derived analogously to Eq. **61**

$$r_{des,[A^*-A^*]} = k_{des}\theta_{A^*}\left[-\frac{2\theta_{A^*-A^*}}{\theta_{A^*}}e^{\frac{\epsilon_{A^*-A^*}}{k_BT}}\Gamma_{des}^3\right] \quad \textbf{[62]}$$

$$r_{des,[A^*-*]} = k_{des}\theta_{A^*}\left[\frac{\theta_{A^*-A^*}}{\theta_{A^*}}e^{\frac{\epsilon_{A^*-A^*}}{k_BT}}\Gamma_{des}^3 - \frac{\theta_{A^*-*}}{\theta_{A^*}}\Gamma_{des}^3\right] \quad \textbf{[63]}$$

$$r_{des,[A^*-A^*]} = k_{des}\theta_{A^*}\left[\frac{2\theta_{A^*-*}}{\theta_{A^*}}\Gamma_{des}^3\right] \quad \textbf{[64]}$$

where the bracketed terms in Eqs. **62** – **64** entirely describe the non-ideal energetic and spatial contributions pertinent to desorption with respect to each ensemble. Eqs. **62** – **64** provide a rigorous description of the kinetic influence of A^*–A^* nearest neighbor interactions on $A_{(g)}$ desorption and include only one independent variable, $\varepsilon_{A^*-A^*}$, not found in the thermodynamically-ideal case. Analogous first-order rate equations are readily derived for any thermodynamically non-ideal one- or two-site elementary step – as is detailed in our prior work [12] – and provide an analytical method by which to reliably account for both combinatorial and thermodynamic non-idealities.

4.3 Incorrect representation of multi-site elementary steps

We address a common misrepresentation of multi-site elementary step events to prevent erroneous application of the first-order truncation procedure. Consider the surface reaction of A^*–A^* pairs adjacent to a vacant site

$$A^* - A^* - * \rightarrow A_{2(g)} + * - * - * \quad \textbf{[65]}$$

occurring with rate $k_{sr}\theta_{A^*-A^*-*}$ which, in the first order, is truncated in terms of one- and two-site ensemble coverages. To ensure appropriate application of the truncation method, we discourage writing this elementary step event as

$$A^* - A^* + * \rightarrow A_{2(g)} + * - * \; + \; * \quad \textbf{[66]}$$

because this representation erroneously suggests the rate of the concerned event may be written as $k_{sr}\theta_{A^*-A^*}\theta_*$ per the law of mass action. This rate expression is incorrect because (i) the event may equivalently be written as

$$A^* + A^* - * \rightarrow A_{2(g)} + * + * - * \qquad \textbf{[67]}$$

giving rate $k_{sr}\theta_{A^*-*}\theta_{A^*} \neq k_{sr}\theta_{A^*-A^*}\theta_*$, and (ii) the coverage of the reacting three-site ensemble is, in actuality, $\theta_{A^*-A^*-*} = \theta_{A^*-A^*}\theta_{A^*-*}/\theta_{A^*}$ following the first order truncation procedure detailed in Section 2.1.

The incorrect rate expressions which follow naturally from Eqs. **66** and **67** highlight the importance of writing multi-site elementary step events in terms of the *entire contiguous ensemble* on which the event occurs – as in Eq. **65**.

4.4 Relation of the described method to density functional theory (DFT) calculations

We stress that this work does not provide an alternative to DFT methods for calculation of elementary step kinetic parameters. Rather, the described methodology is complementary to DFT and serves to improve upon mean-field microkinetic models heretofore employed for the calculation of rates of composite reactions based on DFT-determined initial-state and transition-state energies. DFT calculations provide identical inputs for both higher-order and mean-field (e.g. Langmuir-Hinshelwood) microkinetic models; however, compared to mean-field methods, the higher-order framework more faithfully describes all relevant catalytic phenomena including, but not limited to, ensemble site requirements of elementary steps and surface species, lateral adsorbate interactions, and adsorbate surface diffusion. In this manner, the described formalism provides an alternative to lattice-based kMC simulation – previously the only method capable of simultaneously capturing thermodynamic and combinatorial non-idealities in catalytic surface reactions.

5. Conclusion

Multi-site requirements of elementary steps and/or surface species generally exclude reliability of the Langmuir-Hinshelwood kinetic description which is predicated on a random, uniform distribution of adspecies. Disparate site-size requirements and rates of elementary steps fundamentally engender islanding/partitioning of adsorbates which affects a 'poorly mixed' surface and profoundly influences all kinetic descriptors (e.g. rates, selectivities, and activation energies). Poor 'surface mixing' is only rectified by infinitely-fast surface diffusion if all adspecies occupy a single site; there is no physical condition which generally guarantees validity of the Langmuir-Hinshelwood method to describe catalysis of multi-site occupants (e.g. $^{*}C_nH_m^{*}$ in catalytic hydrogenolysis).

The catalytic consequences of (i) finitely-fast adsorbate diffusion, (ii) multi-site elementary step requirements, (iii) multi-site occupation of surface intermediates, and (iv) lateral adsorbate interactions (i.e. thermodynamic non-idealities) are all incognizable to the Langmuir-Hinshelwood formalism and are rigorously describable by higher-order kinetic theories presented herein. Description of each of these non-ideal phenomena, (i)-(iv), requires ensemble-specific rate terms which quantitatively capture the unique influence each site ensemble exerts on each elementary step – and *vice versa*. Faithful kinetic description of ensemble-specific elementary step events achieved by higher-order analytical methods proffers greater quantitative accuracy and descriptive scope compared to zeroth-order, Langmuir-Hinshelwood methods. In particular, first- and second-order descriptions examined herein reveal (i) relative propagation of competing catalytic reaction paths is dictated by the coverage and biased distribution of prevalent site ensembles, (ii) a single elementary step can, counter-intuitively, be both equilibrated and rate-determining, (iii) adsorbate islanding/partitioning phenomena profoundly influence the physical

interpretation of activation enthalpies and entropies, and (iv) multi-site occupation of surface intermediates confers stringent constraints on adsorbate coverage/distribution which is responsible for the Langmuir-Hinshelwood formalism erroneously calculating non-physical quantities. These observations affirm the need for higher-order analytical methods to generally describe catalytic phenomena and provide an informative, quantitative framework for the kinetic (re-)interpretation of all catalytic reactions proceeding via ≥two-site elementary steps and/or surface species.

Acknowledgements

We dedicate this article to Michel Boudart, whose work, in substance and in style, serves as a foundation and as inspiration for our research.

We thank Zhichen (Jane) Shi for helpful technical discussions and the reviewers for their valuable comments.

This work was funded by the US Department of Energy, Office of Basic Energy Science, Catalysis Science Program (Award DE-SC00019028).

References

[1] C.T. Campbell, B.E. Koel, Chlorine Promotion of Selective Ethylene Oxidation over Ag(110): Kinetics and Mechanism, J. Catal. 92 (1985) 272–283. doi:10.1016/0021-9517(85)90261-1.

[2] C.-J. Chen, J.W. Harris, A. Bhan, Kinetics of Ethylene Epoxidation on a Promoted Ag/α-Al2O3 Catalyst-The Effects of Product and Chloride Co-Feeds on Rates and Selectivity, Chem. Eur. J. 24 (2018) 1–12. doi:10.1002/chem.201801356.

[3] T.C. Wong, L.F. Brown, G.L. Haller, Hydrogenolysis and Hydrogenation of Hydrocarbons on Supported Rh-Ir Bimetallic Catalysts, J. Chem. Soc. Faraday Transcations. 71 (1981) 519–533. doi:10.1039/F19817700519.

[4] M.M. Sullivan, A. Bhan, Effects of oxygen coverage on rates and selectivity of propane-CO_2 reactions on molybdenum carbide, J. Catal. 357 (2018) 195–205. doi:10.1016/j.jcat.2017.11.004.

[5] E. Iglesia, M. Boudart, Structure-Sensitivity and Ensemble Effects In Reactions of Strongly Adsorbed Intermediates. Catalytic Dehydrogenation and Dehydration of Formic Acid on Nickel, J. Phys. Chem. 95 (1991) 7011–7016. doi:10.1021/j100171a053.

[6] C.T. Campbell, M.T. Paffett, A.F. Voter, Testing site size requirements in chemisorption: Experiment and theory, J. Vac. Sci. Technol. A. 4 (1986) 1342–1346. doi:10.1116/1.573608.

[7] R.G. Windham, B.E. Koel, T. Paffett, Studies of the Ensemble Size Requirements for Ethylene Adsorption and Decomposition on Pt(lll): Ethylene and Bismuth Coadsorption, Langmuir. 4 (1988) 1113–1118. doi:10.1021/la00083a009.

[8] G.A. Martin, R. Dutartre, S. Yuan, C. Marquez-Alvarez, C. Mirodatos, Applicability and

Limits of the Ensemble Model in Catalysis by Metals: The Kinetics of Ethane Hydrogenolysis over Pt/SiO_2, J. Catal. 177 (1998) 105–112. doi:10.1006/jcat.1998.2070.

[9] M. Andersen, C.P. Plaisance, K. Reuter, Assessment of mean-field microkinetic models for CO methanation on stepped metal surfaces using accelerated kinetic Monte Carlo, J. Chem. Phys. 147 (2017) 152705. doi:10.1063/1.4989511.

[10] B. Temel, H. Meskine, K. Reuter, M. Scheffler, H. Metiu, Does phenomenological kinetics provide an adequate description of heterogeneous catalytic reactions?, J. Chem. Phys. 126 (2007) 204711. doi:10.1063/1.2741556.

[11] H.C. Kang, W.H. Weinberg, M.W. Deem, Reactant segregation in a Langmuir-Hinshelwood surface reaction, J. Chem. Phys. 93 (1990) 6841–6850. doi:10.1063/1.458916.

[12] N.K. Razdan, A. Bhan, Kinetic description of site ensembles on catalytic surfaces, Proc. Natl. Acad. Sci. 118 (2021) 1–11. doi:10.1073/pnas.2019055118.

[13] C.N. Hinshelwood, Kinetics of chemical change in gaseous systems, Oxford University Press, Oxford, 1926.

[14] J.W. Evans, Kinetic Phase Transitions in Catalytic Reaction Models, Langmuir. 7 (1991) 2514–2519.

[15] M. Boudart, G. Djéga-Mariadassou, Kinetics of Elementary Steps, in: J.M. Prausnitz, L. Brewer (Eds.), Kinet. Heterog. Catal. React., 1st ed., Princeton University Press, Princeton, 1984: pp. 39–77.

[16] T.L. Hill, Introduction to Statistical Thermodynamics, Addison-Wesley, Reading, Massachusetts, 1960.

[17] O.A. Hougen, K.M. Watson, Solid Catalysts and Reaction Rates - General Principles, Ind.

Eng. Chem. 35 (1943) 529–541. doi:10.1021/IE50401A005.

[18] D.W. Flaherty, E. Iglesia, Transition-State Enthalpy and Entropy Effects on Reactivity and Selectivity in Hydrogenolysis of n-Alkanes, J. Am. Chem. Soc. 135 (2013) 18586−18599. doi:10.1021/ja4093743.

[19] J.W. Evans, R.S. Nord, Competitive irreversible random one-, two-, three-, . . . point adsorption on two-dimensional lattices, Phys. Rev. B. 31 (1985) 1759–1769.

[20] J.W. Evans, D.R. Burgess, D.K. Hoffman, Irreversible random and cooperative processes on lattices: Exact and approximate hierarchy truncation and solution, J. Chem. Phys. 79 (1983) 5011–5022. doi:10.1063/1.445595.

[21] R.S. Nord, J.W. Evans, Irreversible immobile random adsorption of dimers, trimers, ... on 2D lattices, J. Chem. Phys. 82 (1985) 2795–2810. doi:10.1063/1.448279.

[22] V.P. Zhdanov, Lattice-gas model of bimolecular reaction on surface, Surf. Sci. Lett. 102 (1981) L35–L40. doi:10.1016/0167-2584(81)90570-3.

[23] Á. Logadóttir, J.K. Nørskov, Ammonia synthesis over a Ru(0001) surface studied by density functional calculations, J. Catal. 220 (2003) 273–279. doi:10.1016/S0021-9517(03)00156-8.

[24] O. Hinrichsen, R. Rosowski, M. Muhler, G. Ertl, The microkinetics of ammonia synthesis catalyzed by cesium-promoted ruthenium, Chem. Eng. Sci. 51 (1996) 1683–1690. doi:10.1016/0009-2509(96)00027-9.

[25] J.W. Evans, D.K. Hoffman, D.R. Burgess, Competing irreversible cooperative adsorption on polymer chains, J. Chem. Phys. 80 (1984) 936–943. doi:10.1063/1.446751.

[26] B.L. Foley, A. Bhan, Degree of rate control and De Donder relations-An interpretation based on transition state theory, J. Catal. 384 (2020) 231–251.

doi:10.1016/j.jcat.2020.02.008.

[27] B.L. Foley, A. Bhan, Thermodynamically consistent forward and reverse degrees of rate control in reversible reactions, J. Catal. 389 (2020) 566–577. doi:10.1016/j.jcat.2020.06.013.

[28] A. Hussain Motagamwala, J.A. Dumesic, Analysis of reaction schemes using maximum rates of constituent steps, Proc. Natl. Acad. Sci. 113 (2016) E2879–E2888. doi:10.1073/pnas.1605742113.

[29] C. Stegelmann, A. Andreasen, C.T. Campbell, Degree of Rate Control: How Much the Energies of Intermediates and Transition States Control Rates, J. Am. Chem. Soc. 131 (2009) 8077–8082. doi:10.1021/ja9000097.

[30] H. Meskine, S. Matera, M. Scheffler, K. Reuter, H. Metiu, Examination of the concept of degree of rate control by first-principles kinetic Monte Carlo simulations, Surf. Sci. 603 (2009) 1724–1730. doi:10.1016/j.susc.2008.08.036.

[31] J.A. Dumesic, Analyses of Reaction Schemes Using De Donder Relations, J. Catal. 185 (1999) 496–505. doi:10.1006/jcat.1999.2523.

[32] Z. Mao, C.T. Campbell, The degree of rate control of catalyst-bound intermediates in catalytic reaction mechanisms: Relationship to site coverage, J. Catal. 381 (2020) 53–62. doi:10.1016/j.jcat.2019.09.044.

[33] C. Reece, R.J. Madix, Moving from Fundamental Knowledge of Kinetics and Mechanisms on Surfaces to Prediction of Catalyst Performance in Reactors, ACS Catal. 11 (2021) 3048–3066. doi:10.1021/acscatal.0c05173.

[34] C.T. Campbell, J.M. Campbell, P.J. Dalton, F.C. Henn, J.A. Rodriguez, S.G. Seimanides, Probing Ensemble Effects in Surface Reactions. 1. Site-Size Requirements for the

Dehydrogenation of Cyclic Hydrocarbons on Pt(111) Revealed by Bismuth Site Blocking, J. Phys. Chem. 93 (1989) 806–814. doi:10.1021/j100339a056.

[35] W.M.H. Sachtler, R.A. van Santen, Surface Composition and Selectivity of Alloy Catalysts, Adv. Catal. 26 (1977) 69–119. doi:10.1016/S0360-0564(08)60070-X.

[36] C. Stegelmann, N.C. Schiødt, C.T. Campbell, P. Stoltze, Microkinetic modeling of ethylene oxidation over silver, J. Catal. 221 (2004) 630–649. doi:10.1016/j.jcat.2003.10.004.

[37] A. Kumar, A. Bhan, Oxygen content as a variable to control product selectivity in hydrodeoxygenation reactions on molybdenum carbide catalysts, Chem. Eng. Sci. 197 (2019) 371–378. doi:10.1016/j.ces.2018.12.027.

[38] C.H. Lien, J.W. Medlin, Promotion of activity and selectivity by alkanethiol monolayers for Pd-catalyzed benzyl alcohol hydrodeoxygenation, J. Phys. Chem. C. 118 (2014) 23783–23789. doi:10.1021/jp507114g.

[39] S. Wang, E. Iglesia, Entropy-Driven High Reactivity of Formaldehyde in Nucleophilic Attack by Enolates on Oxide Surfaces, J. Am. Chem. Soc. 140 (2018) 775–782. doi:10.1021/jacs.7b11749.

[40] W. Tu, Y.-H. (Cathy) Chin, Catalytic Consequences of Chemisorbed Oxygen during Methanol Oxidative Dehydrogenation on Pd Clusters, ACS Catal. 5 (2015) 3375–3386. doi:10.1021/acscatal.5b00068.

[41] K.-I. Fujimoto, F.H. Ribeiro, M. Avalos-Borja, E. Iglesia, Structure and Reactivity of PdOx/ZrO2 Catalysts for Methane Oxidation at Low Temperatures, J. Catal. 179 (1998) 431–442. doi:10.1006/jcat.1998.2178.

[42] W. Tu, M. Ghoussoub, C. Veer Singh, Y.-H. (Cathy) Chin, Consequences of Surface

Oxophilicity of Ni, Ni-Co, and Co Clusters on Methane Activation, J. Am. Chem. Soc. 139 (2017) 6928–6945. doi:10.1021/jacs.7b01632.

[43] N. Cardona-Martinez, J.A. Dumesic, Applications of Adsorption Microcalorimetry to the Study of Heterogeneous Catalysis, Adv. Catal. 38 (1992) 149–244. doi:10.1016/S0360-0564(08)60007-3.

[44] K. Liu, A. Wang, W. Zhang, J. Wang, Y. Huang, X. Wang, J. Shen, T. Zhang, Microkinetic Study of CO Oxidation and PROX on Ir-Fe Catalyst, Ind. Eng. Chem. Res. 50 (2011) 758–766. doi:10.1021/ie1009052.

[45] J. Shen, J.M. Hill, R.M. Watwe, B.E. Spiewak, J.A. Dumesic, Microcalorimetric, infrared spectroscopic, and DFT studies of ethylene adsorption on Pt/SiO_2 and $Pt-Sn/SiO_2$ catalysts, J. Phys. Chem. B. 103 (1999) 3923–3934. doi:10.1021/jp9902452.

[46] J.B. Miller, H.R. Siddiqui, S.M. Gates, J.N. Russell, J.T. Yates, J.C. Tully, M.J. Cardillo, Extraction of kinetic parameters in temperature programmed desorption: A comparison of methods, J. Chem. Phys. 87 (1987) 6725–6732. doi:10.1063/1.453409.

[47] P. Azadi, G. Brownbridge, I. Kemp, S. Mosbach, J.S. Dennis, M. Kraft, Microkinetic modeling of the Fischer-Tropsch synthesis over cobalt catalysts, ChemCatChem. 7 (2015) 137–143. doi:10.1002/cctc.201402662.

[48] R.A. Van Santen, A.J. Markvoort, I.A.W. Filot, M.M. Ghouri, E.J.M. Hensen, Mechanism and microkinetics of the Fischer-Tropsch reaction, Phys. Chem. Chem. Phys. 15 (2013) 17038. doi:10.1039/c3cp52506f.

[49] S. Storsaeter, D. Chen, A. Holmen, Microkinetic modelling of the formation of C_1 and C_2 products in the Fischer-Tropsch synthesis over cobalt catalysts, Surf. Sci. 600 (2006) 2051–2063. doi:10.1016/j.susc.2006.02.048.

[50] S.A. Goddard, R.D. Cortright, J.A. Dumesic, Deuterium Tracing Studies and Microkinetic Analysis of Ethylene Hydrogenation over Platinum, J. Catal. 137 (1992) 186–198. doi:10.1016/0021-9517(92)90148-B.

[51] A.S. McLeod, L.F. Gladden, Monte Carlo simulation of kinetic discontinuities in hydrocarbon hydrogenation reactions, Catal. Letters. 43 (1997) 189–194. doi:10.1023/A:1018923513660.

[52] J.E. Rekoske, R.D. Cortright, S.A. Goddard, S.B. Sharma, J.A. Dumesic, Microkinetic Analysis of Diverse Experimental Data for Ethylene Hydrogenation on Platinum, J. Phys. Chem. 96 (1992) 1880–1888. doi:10.1021/j100183a067.

[53] D. Duca, L. Botar, T. Vidoczy, Monte Carlo Simulation of Ethylene Hydrogenation on Pt Catalysts, J. Catal. 162 (1996) 260–267. doi:10.1006/jcat.1996.0283.

[54] E. Iglesia, S.L. Soled, R.A. Fiato, G.H. Via, Bimetallic Synergy in Cobalt Ruthenium Fischer-Tropsch Synthesis Catalysts, J. Catal. 143 (1993) 345–368. doi:10.1006/JCAT.1993.1281.

[55] A.K. Datye, J. Schwank, Fischer-Tropsch synthesis on bimetallic ruthenium-gold catalysts, J. Catal. 93 (1985) 256–269. doi:10.1016/0021-9517(85)90173-3.

[56] V.P. Zhdanov, Lattice-gas model for description of the adsorbed molecules of two kinds, Surf. Sci. 111 (1981) 63–79. doi:10.1016/0039-6028(81)90475-1.

[57] V.P. Zhdanov, Effect of the lateral interaction of adsorbed molecules on preexponential factor of the desorption rate constant, Surf. Sci. Lett. 111 (1981) L662–L666. doi:10.1016/0167-2584(81)90202-4.

How to write the rate of $A^* + A^*$

$A^* + A^*$ as experienced by $[A^*]$

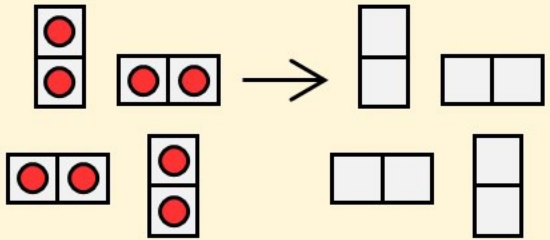

Rate for $[A^*]$ ensemble

$$-\left(\frac{d\theta_{A^*}}{dt}\right)_r = 4k_r\theta_{A^*-A^*}$$

$A^* + A^*$ as experienced by $[A^*–A^*]$

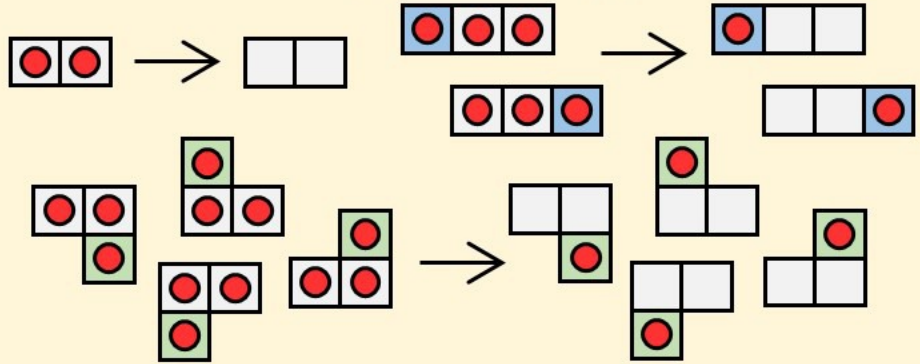

Rate for $[A^*–A^*]$ ensemble

$$-\left(\frac{d\theta_{A^*-A^*}}{dt}\right)_r = k_r\theta_{A^*-A^*} + 2k_r\theta_{A^*-A^*-A^*} + 4k_r\theta_{\substack{A^*-A^* \\ | \\ A^*}}$$

*Color-shaded sites neighbor reactive $A^*–A^*$ pair